Electronic Supplementary Material (ESI) for Materials Chemistry Frontiers.
This journal is © the Partner Organisations 2023

Supplementary information

A Unique Corrole-Based Metal-Organic Polymer for use in Synergistic Phototherapy Treatments

*Wenbo Deng,[a] Meng Jia,[b] Quan Shi,[a] Yunhao Xu,[a] Yaqing Feng,[a] Yanming Zhao,[*c] Min Gong[*d] and Bao Zhang[*a]*

[a] *School of Chemical Engineering and Technology, Tianjin University, Tianjin 300350, China.*

[b] *Xi'an Aerospace Propulsion Test Technology Institute, Xian 710000, China.*

[c] *Henan Institute of Advanced Technology, Zhengzhou University, Zhengzhou 450052, China.*

[d] *College of Pharmacy, Tianjin Medical University, Tianjin 300110, China.*

Corresponding Author

***Yanming Zhao-**Henan Institute of Advanced Technology, Zhengzhou University, China; E-mail: yanmingzhao@zzu.edu.cn

***Min Gong**-College of Pharmacy, Tianjin Medical University, Tianjin 300110, China; E-mail: gongmin@tmu.edu.cn

***Bao Zhang**-School of Chemical Engineering and Technology, Tianjin University, Tianjin 300350, China; E-mail: baozhang@tju.edu.cn

Experimental Sections

Synthesis

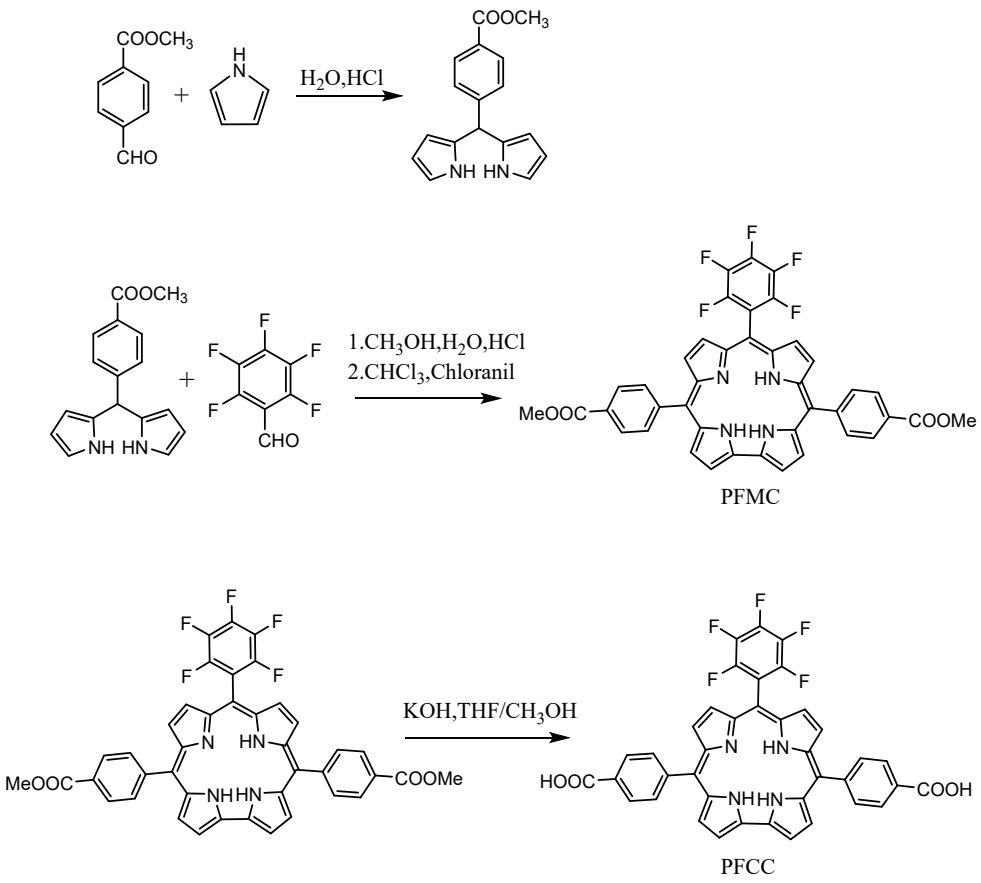

Scheme 1 Synthesis of the corrolic ligand 10-pentafluorophenyl-5,15-di(*p*-carboxyphenyl)corrole (PFCC).

Synthesis of 5-(4-methoxycarbonyl-phenyl)dipyrromethene

5-(4-methoxycarbonyl-phenyl)dipyrromethene has been synthesized on the modification of procedure reported in the literature [1, 2]. 300 mL deionized water, 3 mL HCl and 15 mL freshly evaporated pyrrole (216 mmol) were mixed in a 500 mL two-necked flask at room temperature (25℃). Then, slowly add 100 ml ethanol containing 1.5 g methyl 4-formylbenzoate (9.31mmol)

drop by drop to the two-necked flask under constant pressure. The reaction was then stirred for 30 min, followed by the addition of $NaHCO_3$ to adjust the pH $\geqslant$ 7 at the end of the reaction. Filter the solution, and wash the filter cake with abundant deionized water, and then dry it to obtain white solid. The crude product was subjected to silica chromatography (elution solvent CH_2Cl_2) to afford 1.2g pure white solid with a yield of 64.4%. ^{1}H NMR (600 MHz, DMSO-d_6) δ 10.57 (s, 2H), 7.83 (d, J = 8.3 Hz, 2H), 7.25 (d, J = 8.3 Hz, 2H), 6.65 – 6.50 (m, 2H), 5.86 (q, J = 2.7 Hz, 2H), 5.62 (q, J = 2.8, 2.3 Hz, 2H), 5.40 (s, 1H), 3.78 (s, 3H).

Synthesis of PFMC

10-pentafluorophenyl-5,15-di(4-methoxycarbonyl-phenyl)corrole (PFMC) has been synthesized on the modification of procedure reported in the literature [3]. In a typical procedure, 1.12 g (5.29 mmol) of 5-(4-methoxycarbonyl-phenyl)dipyrromethene was dissolved in 200 mL methanol and 200 mL deionized water at room temperature. Subsequently, 413 μL (2.65 mmol) of pentafluoro-benzaldehyde and 10 mL HCl were added to the reaction system for 4h string in dark. Chloroform was used for extracting reaction solution, which was washed in turn with deionized water and NaCl solution and dried with $NaSO_4$.Then, 1.48 g (6.02 mmol) of tetra-chloro-benzoquinone was then added and stirred overnight in dark at room temperature. After the end of the reaction, the chloroform was removed by evaporation under reduced pressure and further purified by column chromatography (300-400 mesh) silica gel (elution solvent CH_2Cl_2: Petroleum ether = 3:1). The crude product was recrystallized from dichloromethane and petroleum ether, after which the product was washed with methanol and dried to give 479mg purple powder in 24.7% yield. ^{1}H NMR (400 MHz, $CDCl_3$) δ 8.96 (d, J = 4.2 Hz, 1H), 8.91 (d, J = 4.8 Hz, 1H), 8.56 (d, J = 4.3 Hz, 1H), 8.49 (d, J = 7.8 Hz, 3H), 8.42 (d, J = 7.9 Hz, 2H), 4.10 (s, 3H). UV-Vis (CH_2Cl_2)

λmax: 421, 581, 616, 653 nm; MALDI-TOFMS: m/z calculated for $C_{41}H_{25}F_5N_4O_4$, 732.1874; found, 732.985 $[M+H]^+$.

Synthesis of PFCC

In a typical procedure, 100 mg of PFMC was dissolved in solvent mixture of methanol and THF (CH_3OH: THF = 2:1), to which a solution of KOH (287 mg) in 12 mL deionized water was added. After heating the mixture for 48 h at 45℃ under nitrogen atmosphere, the reaction fluid was evaporated to dryness. 300 mL deionized water was then introduced, after which the pH of the solution was adjusted to 7 with HCl (1 M) to precipitate dark green solid from system. The crude product was washed with deionized water and dichloromethane, then dried to obtain 88.6 mg purple-black solid in 92.1% yield. ^{1}H NMR (400 MHz, DMSO-d_6) δ 13.23 (s, 2H), 9.09 (s, 2H), 8.89 (s, 2H), 8.70 (s, 2H), 8.44 (s, 8H), 5.76 (s, 2H), -2.70 (s, 3H). ^{19}F NMR (565 MHz, DMSO-d_6) δ -139.17 (s, 2F), -155.26 (s, 1F), -163.29 (s, 2F). UV-Vis (DMF) λmax: 446, 545, 591, 641 nm; MALDI-TOF MS: m/z calculated for $C_{39}H_{21}F_5N_4O_4$, 704.1518; found, 703.251 $[M-H]^+$.

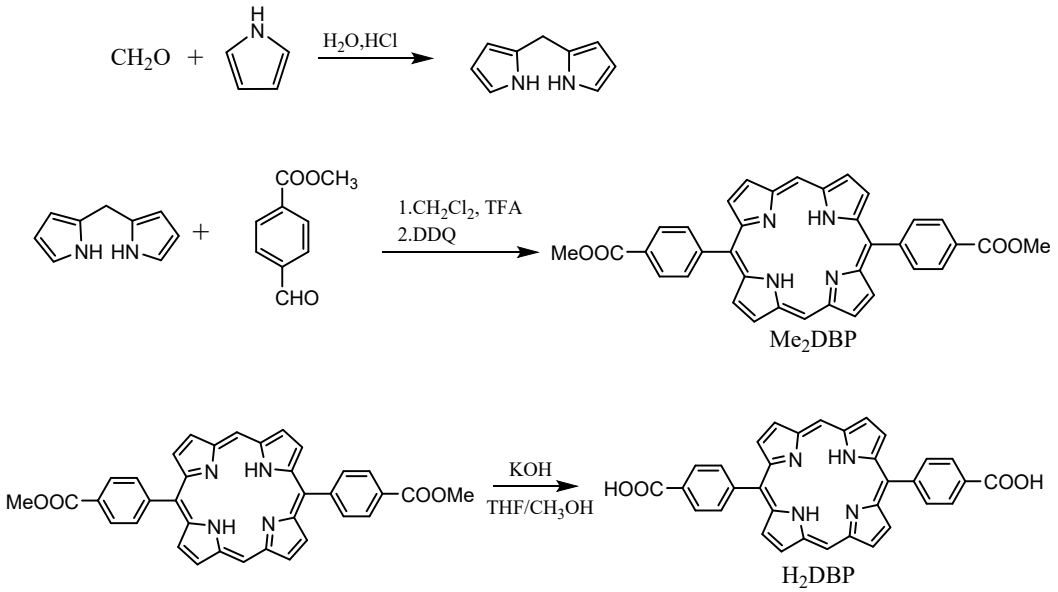

Scheme 2 Synthesis of the porphyrin ligand 5, 15-di(p-benzoato)porphyrin (H_2DBP)

Synthesis of 5, 15-di(p-benzoato)porphyrin

Porphyrin ligand H_2DBP has been successfully synthesized according to the literature reported by Lin's group [4]. Me_2DBP: ^{1}H NMR (400 MHz, Chloroform-*d*) δ 10.37 (s, 2H), 9.44 (d, *J* = 4.2 Hz, 4H), 9.11 – 9.00 (m, 4H), 8.51 (d, *J* = 6.9 Hz, 4H), 8.37 (d, *J* = 7.0 Hz, 4H), 4.15 (s, 6H), -3.14 (s, 2H); MALDI-TOF-MS: m/z calculated for $C_{36}H_{26}N_4O_4$, 578.2049; found, 578.870 $[M+H]^+$. H_2DBP: ^{1}H NMR (400 MHz, DMSO-d_6) δ 13.35 (s, 2H), 10.71 (s, 2H), 9.71 (d, *J* = 4.7 Hz, 4H), 9.08 (d, *J* = 4.7 Hz, 4H), 8.85 – 8.09 (m, 8H), -3.27 (s, 2H); MALDI-TOF-MS: m/z calculated for $C_{34}H_{22}N_4O_4$, 550.1628; found, 551.132 $[M+H]^+$.

Synthesis of PFCC-Hf

PFCC (13.2 mg, 0.018 mmol) and $HfCl_4$ (5.9 mg, 0.018 mmol) were dissolved in 2 mL of DMF solution, followed by adding 0.2 mL of acetic acid as well as 0.15 mL of water. The mixture was sonicated into solution before being put to a 5 mL reaction kettle and heated at 120°C for 72 h. The resulting product was obtained by centrifugation after cooling to ambient temperature, washed with DMF until the top clear layer was colorless, and then dried under vacuum at 100 °C for 12 h to produce black-purple solid. The solid was dispersed in acetone for 48 h, after which it was centrifuged and dried at 100 °C under vacuum for another 12 h to obtain 10mg of nanoscale metal-organic polymers PFCC-Hf.

Synthesis of DBP-Hf

The synthesis procedure of DBP-Hf was modified based on the literature reported by Lin's group [4]. In a typical procedure, H_2DBP (6.9mg, 0.0125 mmol) and $HfCl_4$ (3.9 mg, 0.0125 mmol) were dissolved in 1.6 mL of DMF solution, followed by adding 0.16 mL of trifluoroacetic acid and 0.15 mL of water. The mixture was sonicated into solution before being put to a 5 mL reaction

kettle and heated at 130°C for 72 h. The resulting product was obtained by centrifugation after cooling to ambient temperature, washed with DMF until the top clear layer was colorless, and then dried under vacuum at 100°C for 12 h to produce dark red solid. The solid was dispersed in acetone for 48 h, after which it was centrifuged and dried at 100°C under vacuum for another 12 h to obtain DBP-Hf.

Synthesis of PFCC-Hf@PEG and DBP-Hf@PEG

Both PFCC-Hf and DBP-Hf were modified with HOOC-PEG-COOH according to the article reported [5]. As an example of the PEG modification of PFCC-Hf, 2 mL of aqueous HOOC-PEG-COOH solution (5 mg/mL) was added dropwise to 10 mL PFCC-Hf aqueous dispersion (1 mg/mL). After the mixture was stirred for 1 h in dark, PFCC-Hf@PEG was obtained by sequential centrifugation, washing with deionized water and freeze-drying. The synthesis of DBP-Hf@PEG were the same as the above steps

Material Performance Testing

Light-induce $^1O_2$ generation measurements

To compare the photodynamic efficiency of PFCC-Hf and DBP-Hf, 1,3-diphenylisobenzofuran (DPBF) was used as a singlet oxygen indicator to indirectly characterize the photogenerated singlet oxygen capacity of two nanomaterials. In a typical process, 30 μL of DMF solutions containing DPBF (1 mg/mL) were added into 2 mL PFCC-Hf/DBP-Hf aqueous dispersion (200, 100, 50 μg/mL). After deducting material solution background, the UV absorption spectra of the blended DPBF solutions were examined per minute after external a 660 nm (0.15 W/cm^2) / 505 nm (0.05 W/cm^2) laser irradiation with 15 cm height above the liquid level. In

addition, to exclude the interference of the laser itself as well as absorption disruptions of the porous material, the DPBF group under laser irradiation alone and PFCC-Hf/DBP-Hf with DPBF in dark were set up.

Besides, singlet oxygen quantum yields ΦΔ of PFCC-Hf, DBP-Hf, PFCC, DBP were measured according to reported research with 5,10,15,20-tetraphenylporphyrin (TPP) as the reference ($\Phi_{\Delta}^{R} = 0.64$) [6, 7]. Singlet oxygen quantum yield calculating formula is shown below:

$$\Phi_{\Delta}^{S} = \Phi_{\Delta}^{R} \frac{k^{S} F^{R}}{k^{R} F^{S}}$$

where k^S and k^R respectively represents the slope of absorbance decrease at 420 nm of DPBF solution adding sample materials or reference TPP during laser irradiation. The correction factor F was calculated by the equation: $F = 1\text{-}10^{-OD}$, where OD is the absorbance at 660 nm of sample. The solution concentration of both the sample and the reference was 10 μM. The UV-absorbance of solution were tested after every 1min irradiation of the 660 nm laser.

Photothermal ability test

Irradiate 1 mL of PFCC-Hf, DBP-Hf, PFCC aqueous dispersion by using an 808 nm laser emitter with different power at height of about 15 cm from the liquid surface. To determine the photostability of PFCC-Hf, repeated four times for ten minutes of laser exposure to the PFCC-Hf aqueous dispersion, followed by cooling to room temperature. The photothermal conversion efficiency (PCE) was calculated using the equation reported by Roper [8] and shown below:

$$\eta = \frac{hA(T_{max} - T_{surr}) - Q_{dis}}{I(1 - 10^{-A_{\lambda}})} \quad (1)$$

Where η is the photothermal conversion efficiency. T_{max} is the maximum temperature reached when the sample was irradiated by the laser. T_{surr} is the room temperature. Q_{dis} is the heat absorbed by the sample itself under laser irradiation. A_λ is the absorbance of the same concentration of sample at the wavelength of the corresponding laser. *I* is the power of the laser used. The equation for the parameter hA in (1) is shown below:

$$hA = \frac{m_D C_D}{\tau_s} \quad (2)$$

Where m_D is the mass of the sample to be measured. C_D is the specific heat capacity of the sample to be measured. Time parameters τ_S in equation (2) can be calculated using the following equation:

$$t = -\tau_s ln\theta = -\tau_s \ln\left(\frac{T - T_{surr}}{T_{max} - T_{surr}}\right) \quad (3)$$

Where *t* is the sample cooling time. *T* is the real-time temperature of sample during cooling time after being heated up to maximum temperature.

Drug loading capacity of PFCC-Hf experiment

The standard curve of DOX concentrations was plotted by measuring UV absorbance of DOX aqueous solution at 480 nm. PFCC-Hf (200 μg/mL) in deionized water was stirred with different concentration of DOX (100, 150, 200, 250, 300, 350, 400 μg/mL) for 12 h without light. The PFCC-Hf/DOX was recovered after centrifugation and washed with ultrapure water. The loading capacity of PFCC-Hf for DOX was determined by testing the absorbance of the supernatant at 480 nm after centrifugation. The formulae for calculating the drug loading rate (DLR) and drug entrapment efficiency (DEE) of PFCC-Hf for DOX are shown below:

$$DLR = \frac{\omega - \omega_1}{\omega_{total}} \times 100\%$$

$$DEE = \frac{\omega - \omega_1}{\omega} \times 100\%$$

where ω is the total mass of DOX incorporated. ω_1 is the mass of DOX remaining in the mixture. ω_{total} is the total mass of DOX and PFCC-Hf.

Cell culture

Human malignant melanoma cells A375cells were cultured at 37°C under 5% CO_2 in air with high-glucose DMEM which contained 1% antibiotics and 10% fetal bovine serum. Generally, the media was changed every 2 days, and the cells were digested by trypsin and resuspended in fresh complete medium.

Cellular uptake test by fluoresce imaging

The uptake of PFCC-Hf NMOP nanomaterials by cells was investigated by red fluorescence imaging of PFCC-Hf@PEG/DOX. In particular, the PFCC-Hf@PEG/DOX was prepared in the same way as described above using a concentration of 200 μg/ml for PFCC-Hf@PEG and DOX. A375 cells were incubated with 10 μL hoechst and 500 μL of 200 μg/ml of PFCC-Hf@PEG/DOX medium (solvent PBS: DMEM = 1:3) for 2, 4, 6, 8 h respectively. Hoechst displayed blue fluorescence (ex:360 nm, em:450 nm) in fluorescent microscopy to locate the nucleus of cell while PFCC-Hf@PEG/DOX show red fluorescence (ex:450 nm, em:600 nm) to determine the uptake of cells. This experiment used 24-well plates to culture cells and perform experiments when the cell density reached 10^5/mL.

In vitro cytotoxicity

To assess the biosafety of PFCC-Hf nanomaterials, we firstly tested cellular dark toxicity tests of it. In experiment, A375 cells were feed with 100 μL PFCC-Hf@PEG with various concentration (solvent PBS: DMEM = 1:3) for 24 h. After washing the well 3 times with PBS, 10 μL of CCK8 was added and incubated for 2 h. The final assessment of cell viability was calculated by measuring the OD at 450 nm on enzyme marker.

For phototherapy, PFCC-Hf and DBP-Hf have been selected to investigate the phototherapy effects on cancer cells. First, the A375 cells were divided into 6 groups: (1) PBS, (2) PFCC-Hf / DBP-Hf, (3) PFCC-Hf / DBP-Hf+ 660 nm (4) PFCC-Hf / DBP-Hf+ 808 nm and (5) PFCC-Hf/DBP-Hf+ 808 nm + 660 nm. Subsequently, 100 μL of PBS or PFCC-Hf@PEG / DBP-Hf@PEG with different concentration dispersed in PBS were added to the wells. After 6 h of incubation, cells in the wells were washed 3 times with PBS. Afterwards, the different groups of cells were treated differently, where 660 nm or 808nm meant 3 min 660 nm irradiation or 3 min 808 nm laser irradiation correspondingly. The cell viability test is carried out in the same way as the dark toxicity test shown above. These two experiments used 96-well plates to culture cells and perform experiments when the cell density reached 10^5/mL.

In vitro singlet oxygen detection and AM-PI cell staining

The photodynamic effect of PFCC-Hf in cells was assayed using DFCH-DA as a $^1O_2$ probe. First of all, the A375 cells were divided into 5 groups: (1) PBS, (2) PFCC-Hf, (3) PFCC-Hf + 660 nm (4) PFCC-Hf + 808 nm and (5) PFCC-Hf + 808 nm + 660 nm. Then, 500 μL of PBS or PBS

with PFCC-Hf@PEG (200 μg/mL) were added to the wells. Cells were incubated for 6 h and then treated with laser irradiation (the irradiation time was the same as in the cytotoxicity experiment). Then, 10 μL DFCH-DA solution was added and incubated for 15min, followed by observation by fluorescence microscopy. The AM-PI cell staining experiment was performed as described above except that the DFCH-DA was replaced with AM/PI stain. These two experiments used 24-well plates to culture cells and perform experiments when the cell density reached 10^5/mL

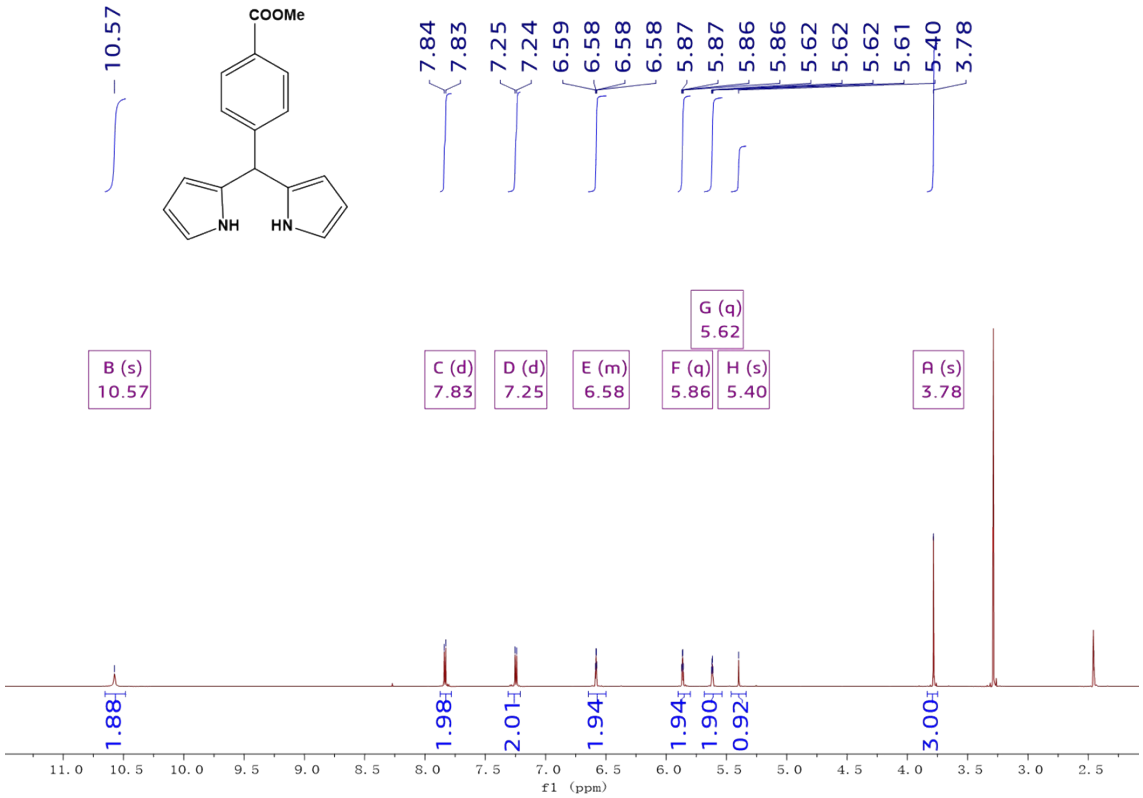

Figure S1 ^{1}H NMR spectrum of 5-(4-methoxycarbonyl-phenyl)dipyrromethene in DMSO-d_6. ^{1}H NMR (600 MHz, DMSO-*d6*) δ 10.57 (s, 2H), 7.83 (d, J = 8.3 Hz, 2H), 7.25 (d, J = 8.3 Hz, 2H), 6.65 – 6.50 (m, 2H), 5.86 (q, J = 2.7 Hz, 2H), 5.62 (q, J = 2.8, 2.3 Hz, 2H), 5.40 (s, 1H), 3.78 (s, 3H).

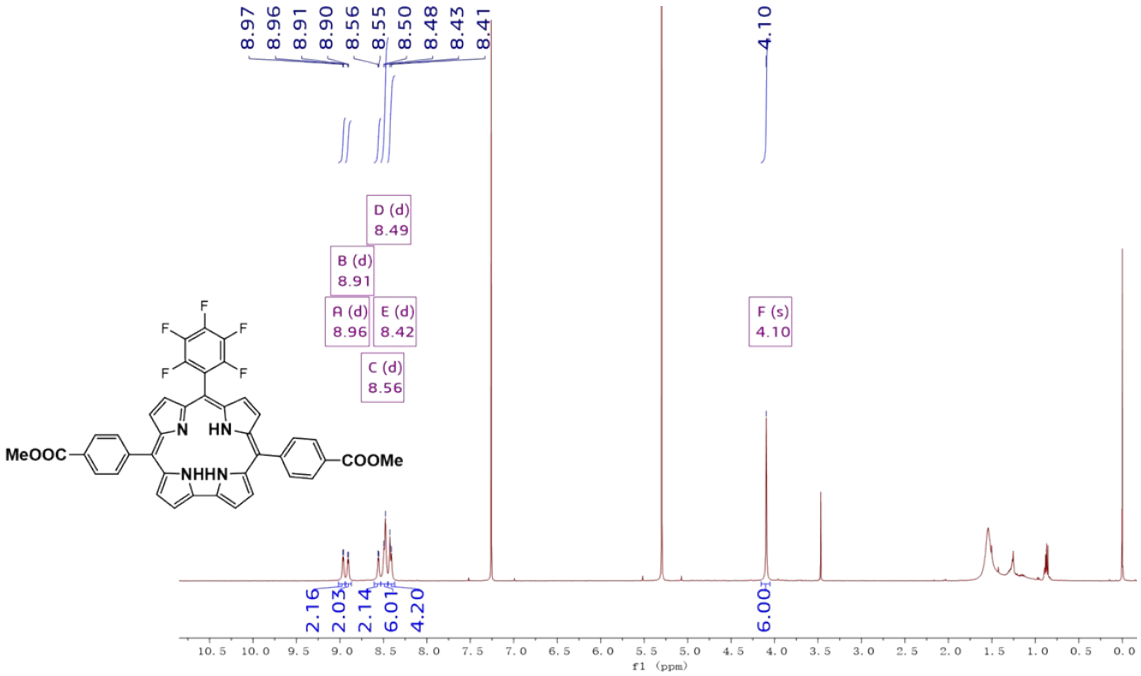

Figure S2 ^{1}H NMR spectrum of PFMC in $CDCl_3$. ^{1}H NMR (400 MHz, $CDCl_3$) δ 8.96 (d, J = 4.2 Hz, 1H), 8.91 (d, J = 4.8 Hz, 1H), 8.56 (d, J = 4.3 Hz, 1H), 8.49 (d, J = 7.8 Hz, 3H), 8.42 (d, J = 7.9 Hz, 2H), 4.10 (s, 3H).

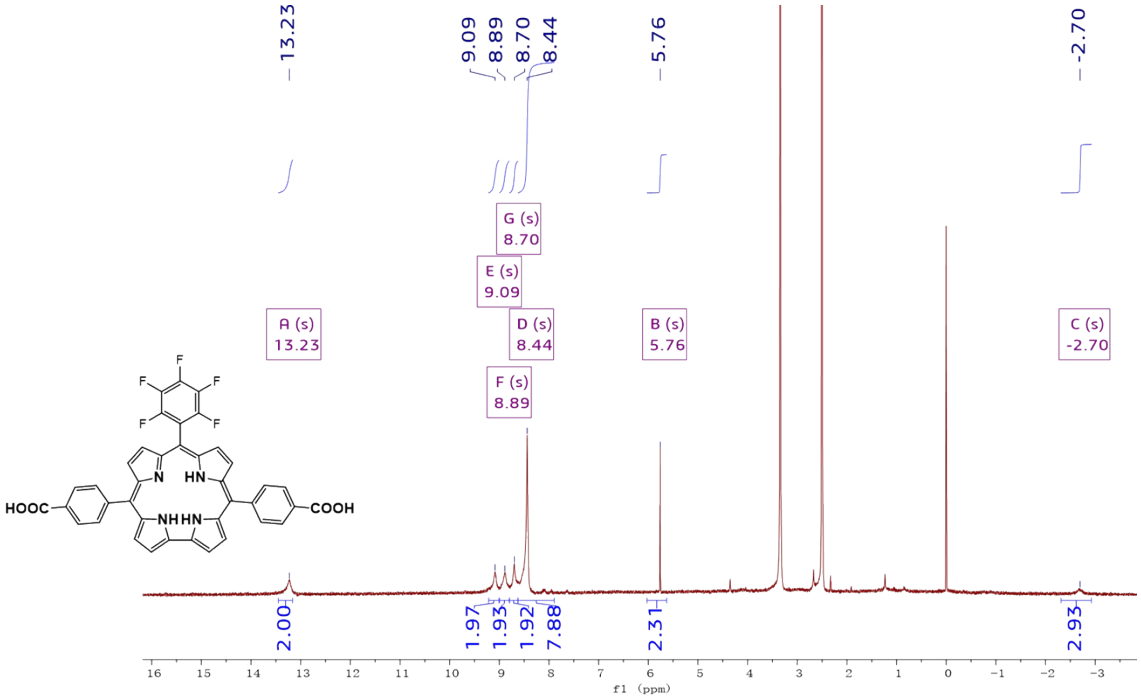

Figure S3 ^{1}H NMR spectrum of PFCC in DMSO-D_6. ^{1}H NMR (400 MHz, DMSO-*d*6) δ 13.23 (s, 2H), 9.09 (s, 2H), 8.89 (s, 2H), 8.70 (s, 2H), 8.44 (s, 8H), 5.76 (s, 2H), -2.70 (s, 3H).

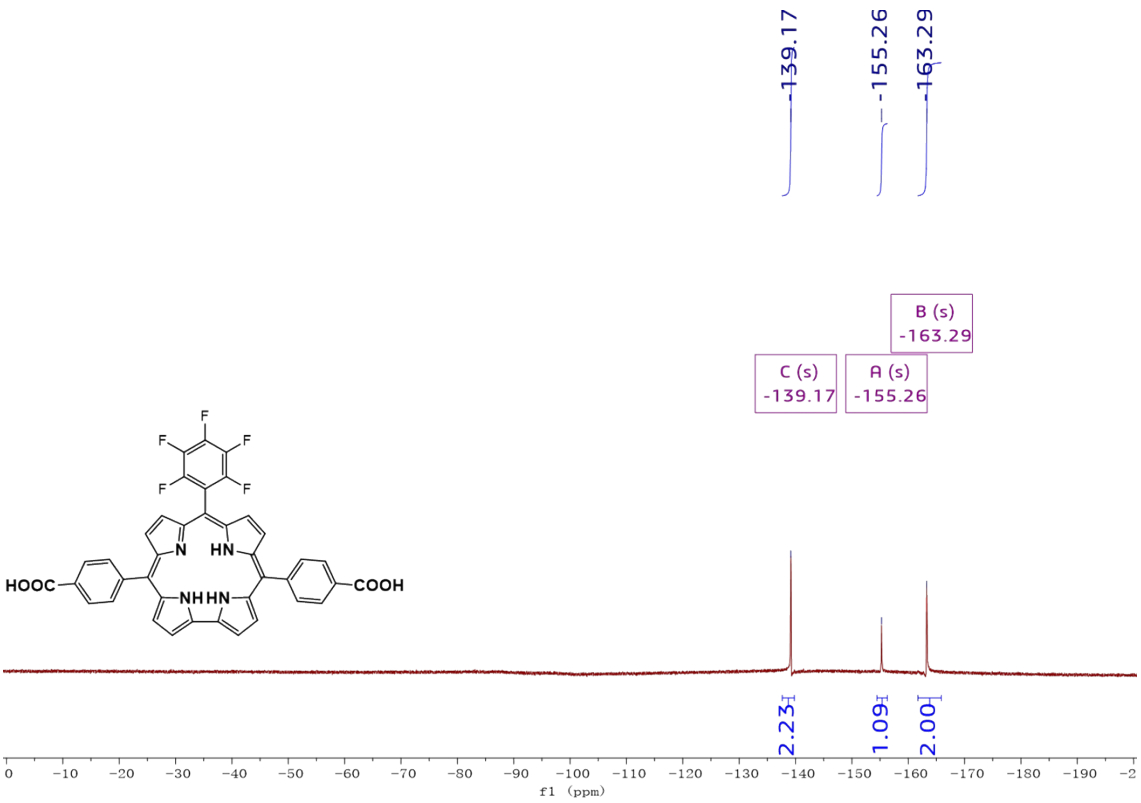

Figure S4 ^{19}F. NMR spectrum of PFCC in DMSO-D$_{6.}$ ^{19}F NMR (565 MHz, DMSO-d_6) δ -139.17 (s, 2F), -155.26 (s, 1F), -163.29 (s, 2F).

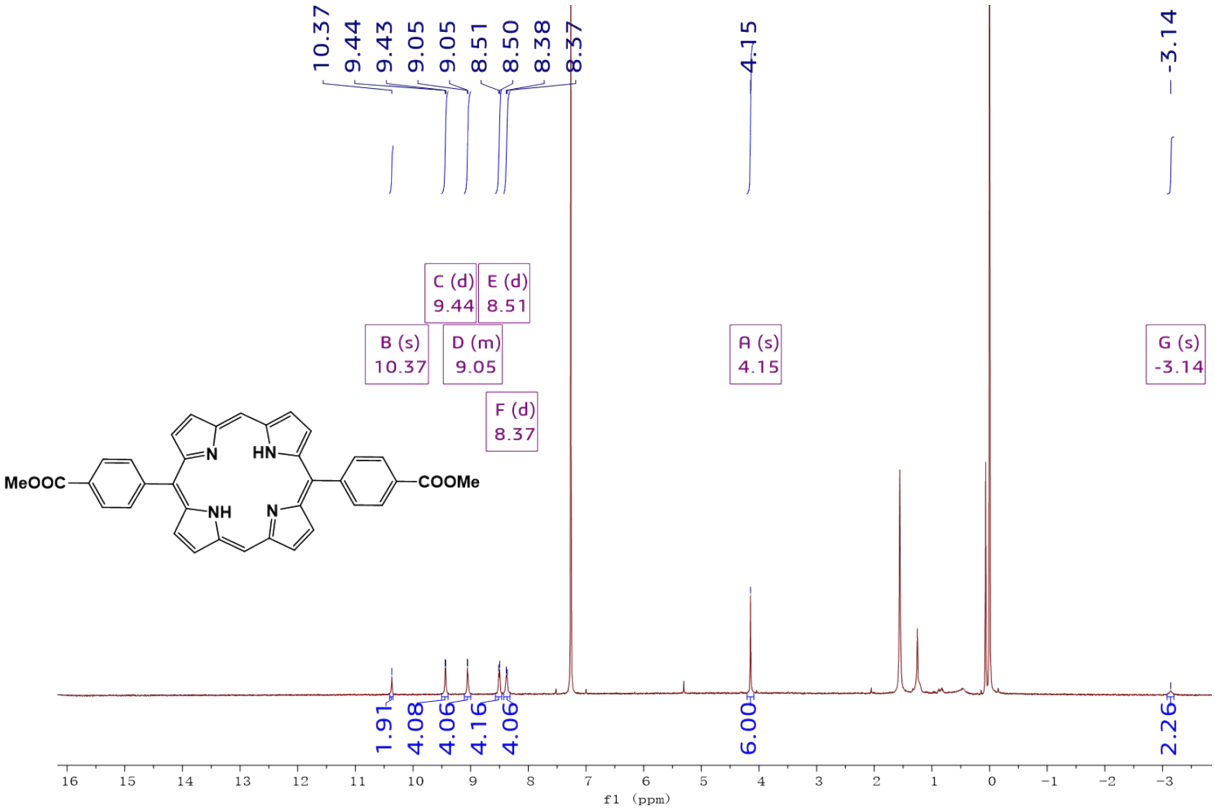

Figure S5 ^{1}H NMR spectrum of Me_2DBP in $CDCl_3$. ^{1}H NMR (400 MHz, Chloroform-*d*) δ 10.37 (s, 2H), 9.44 (d, *J* = 4.2 Hz, 4H), 9.11 – 9.00 (m, 4H), 8.51 (d, *J* = 6.9 Hz, 4H), 8.37 (d, *J* = 7.0 Hz, 4H), 4.15 (s, 6H), -3.14 (s, 2H).

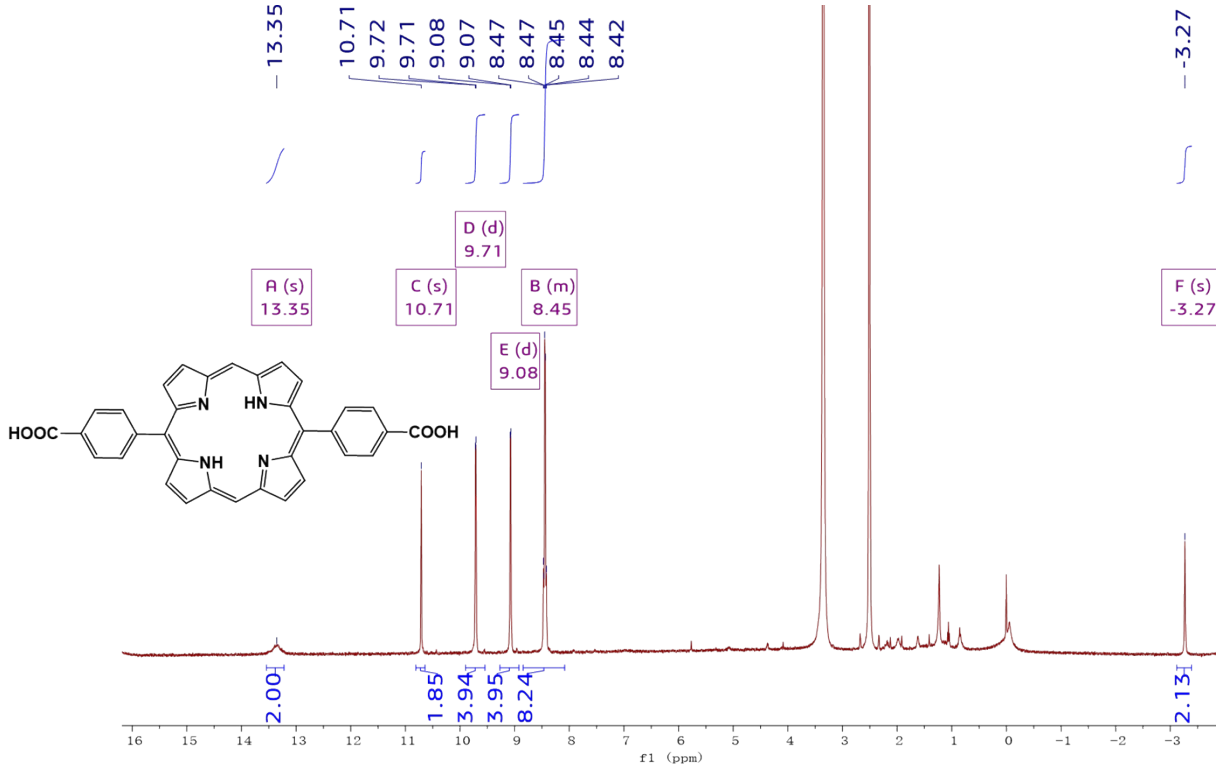

Figure S6 ^{1}H NMR spectrum of H_2DBP in DMSO-D_6. H_2DBP: ^{1}H NMR (400 MHz, DMSO-d_6) δ 13.35 (s, 2H), 10.71 (s, 2H), 9.71 (d, J = 4.7 Hz, 4H), 9.08 (d, J = 4.7 Hz, 4H), 8.85 – 8.09 (m, 8H), -3.27 (s, 2H)

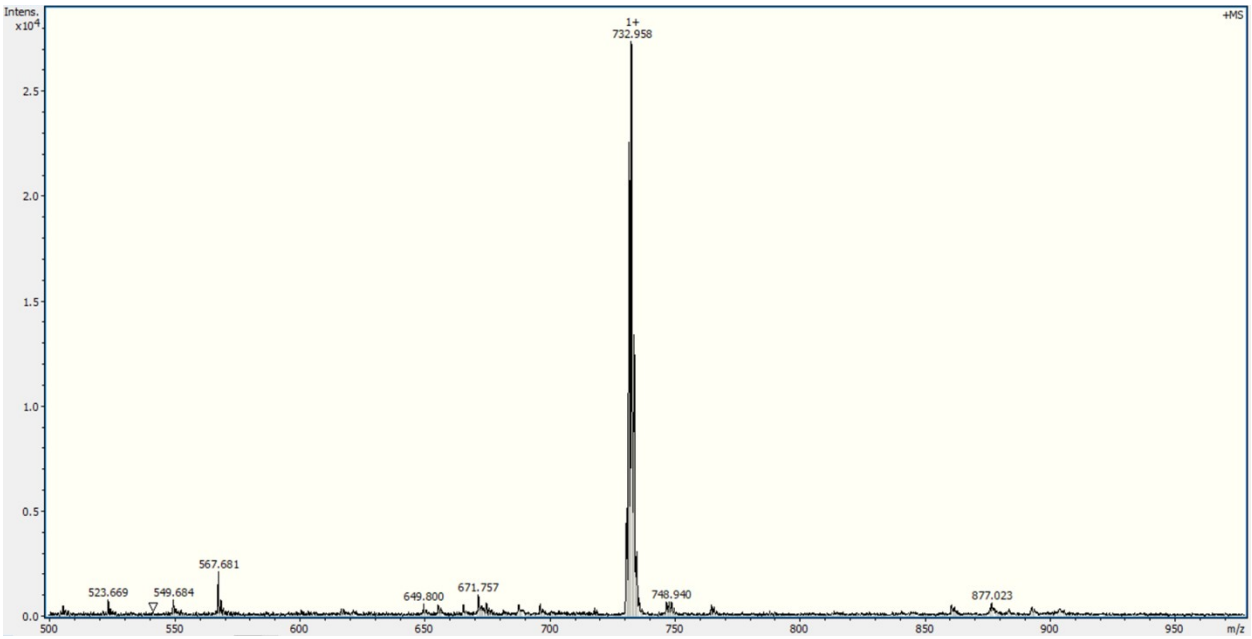

Figure S7 MALDIF-TOF of PFMC, $[PFMC+H]^+$: 732.2 calculated, 733.0 found

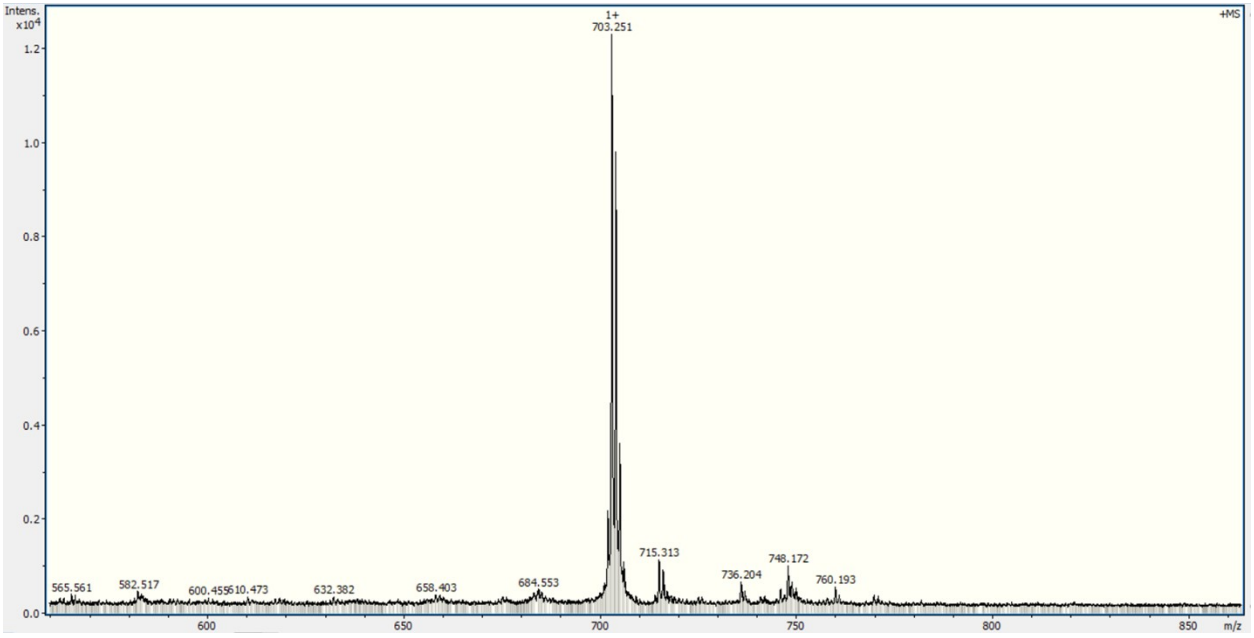

Figure S8 MALDIF-TOF of PFCC, $[PFCC-H]^+$: 704.2 calculated, 703.3 found.

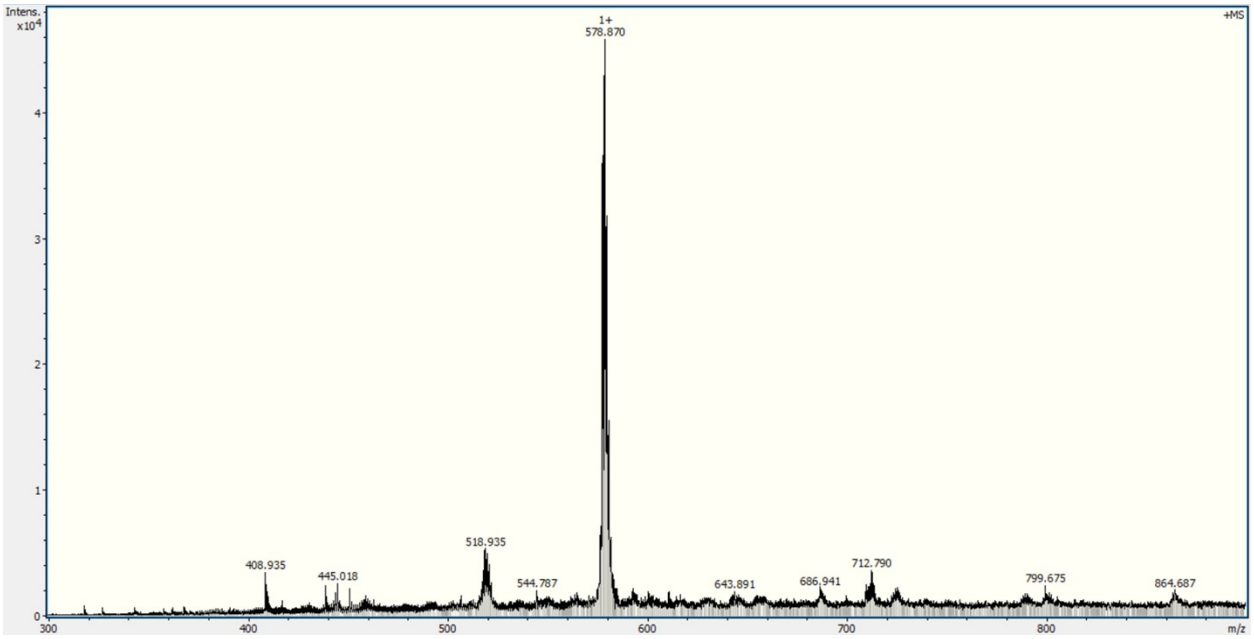

Figure S9 MALDIF-TOF of Me_2DBP, $[Me_2DBP+H]^+$: 578.2 calculated, 578.9 found.

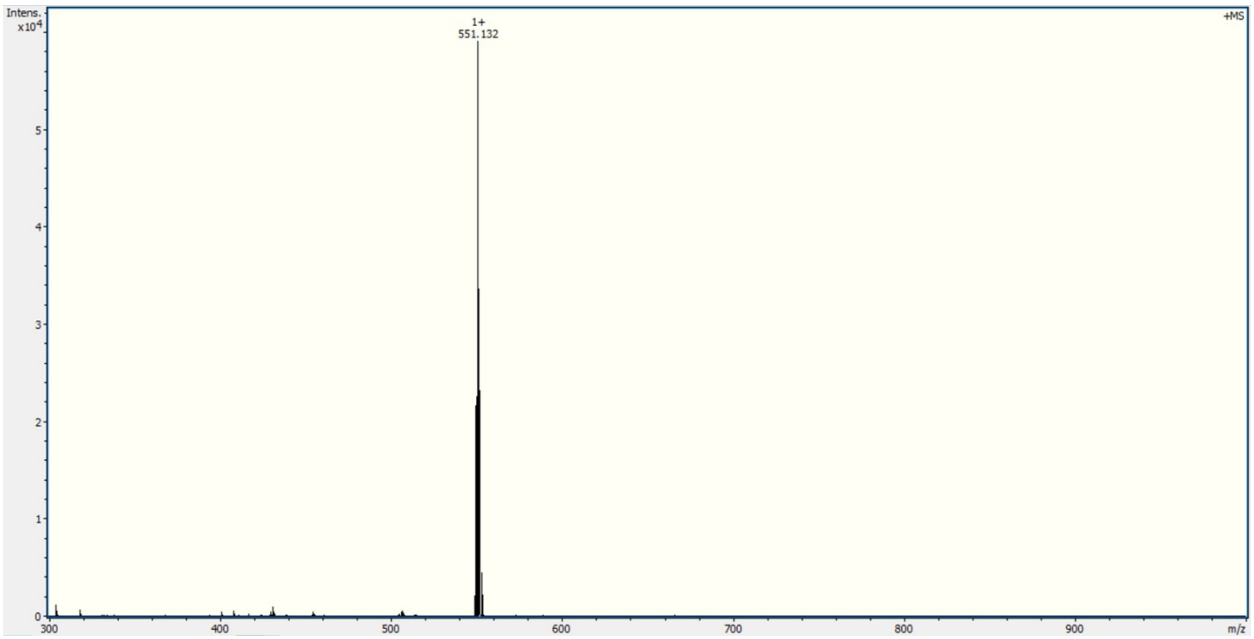

Figure S10 MALDIF-TOF of H_2DBP, $[H_2DBP+H]^+$: 550.2 calculated, 551.1 found.

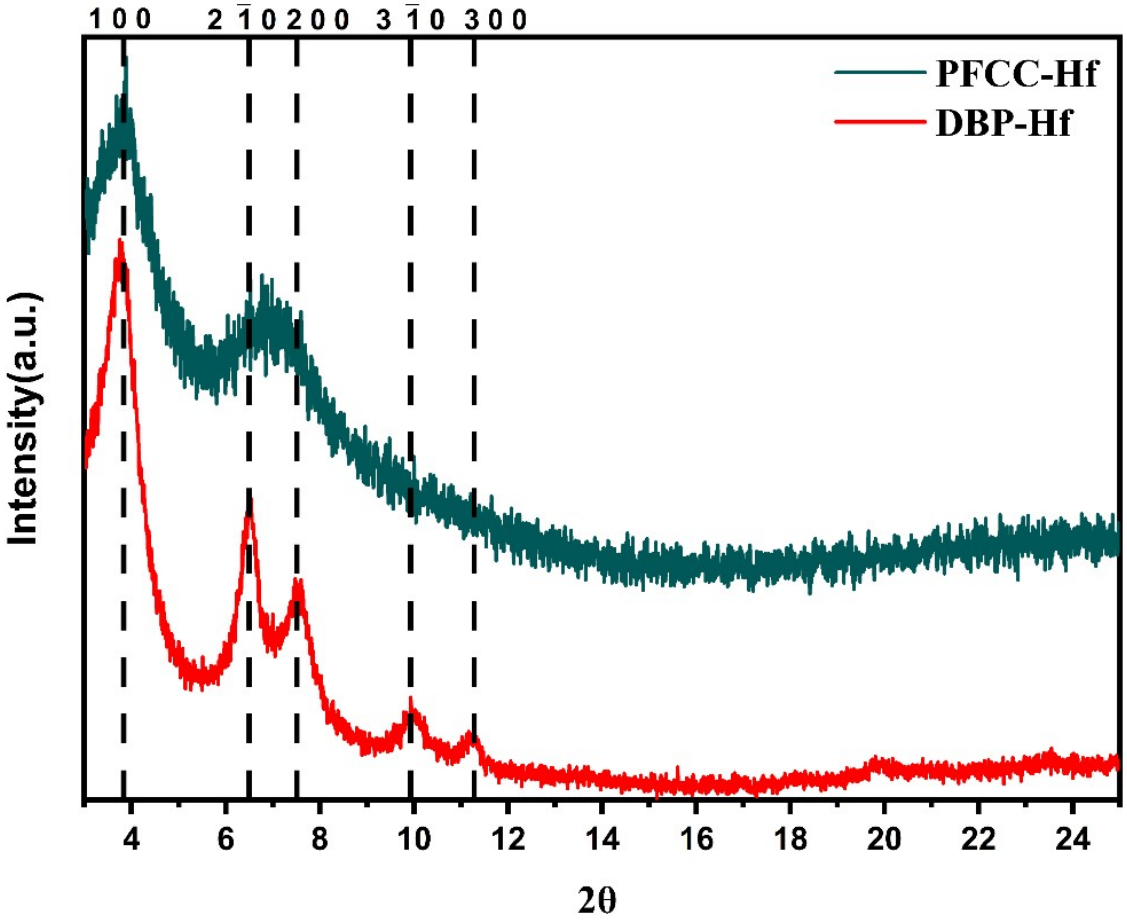

Figure S11 The PXRD comparison of PFCC-Hf and DBP-Hf.

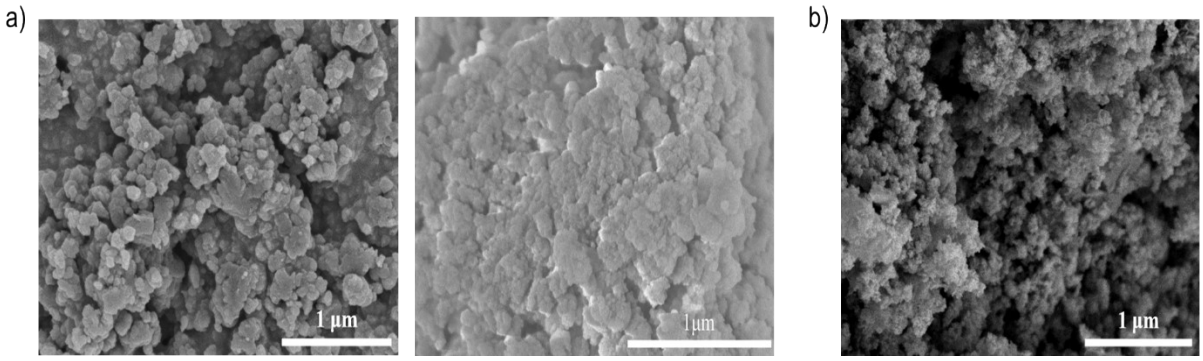

Figure S12 SEM images of a) PFCC-Hf and b) DBP-Hf.

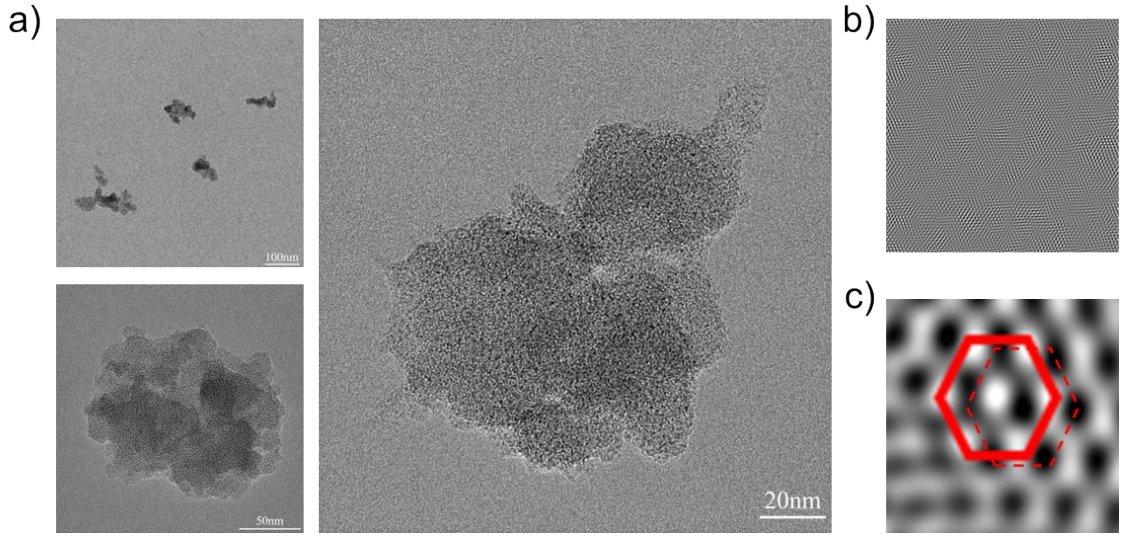

Figure S13 a) High-resolution TEM images of PFCC-Hf at different magnifications. b) Inverse fast Fourier transform (FFT) of TEM image of PFCC-Hf and, c) the enlarged image shows the structure of the 001-crystal plane of PFCC-Hf.

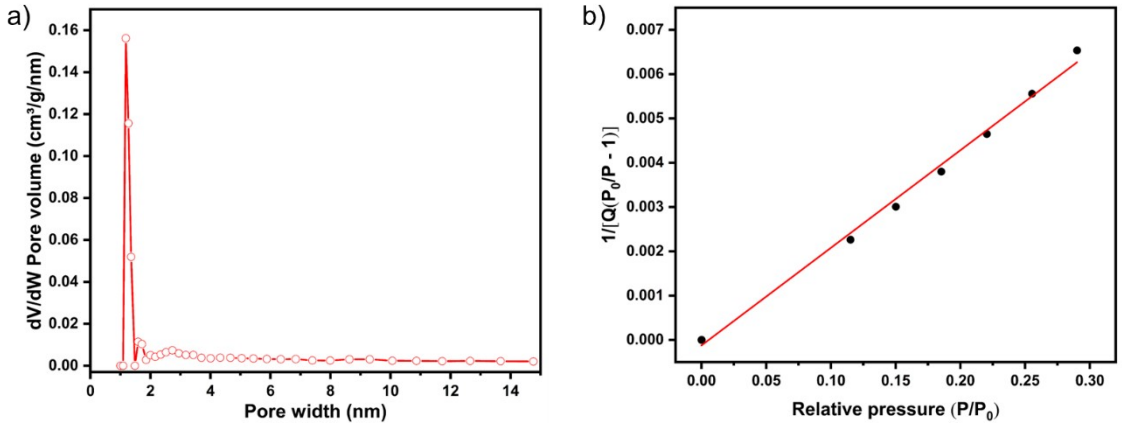

Figure S14 a) Pore size distribution of metal-organic polymers PFCC-Hf. (b) Multiple BET fitting curve of PFCC-Hf.

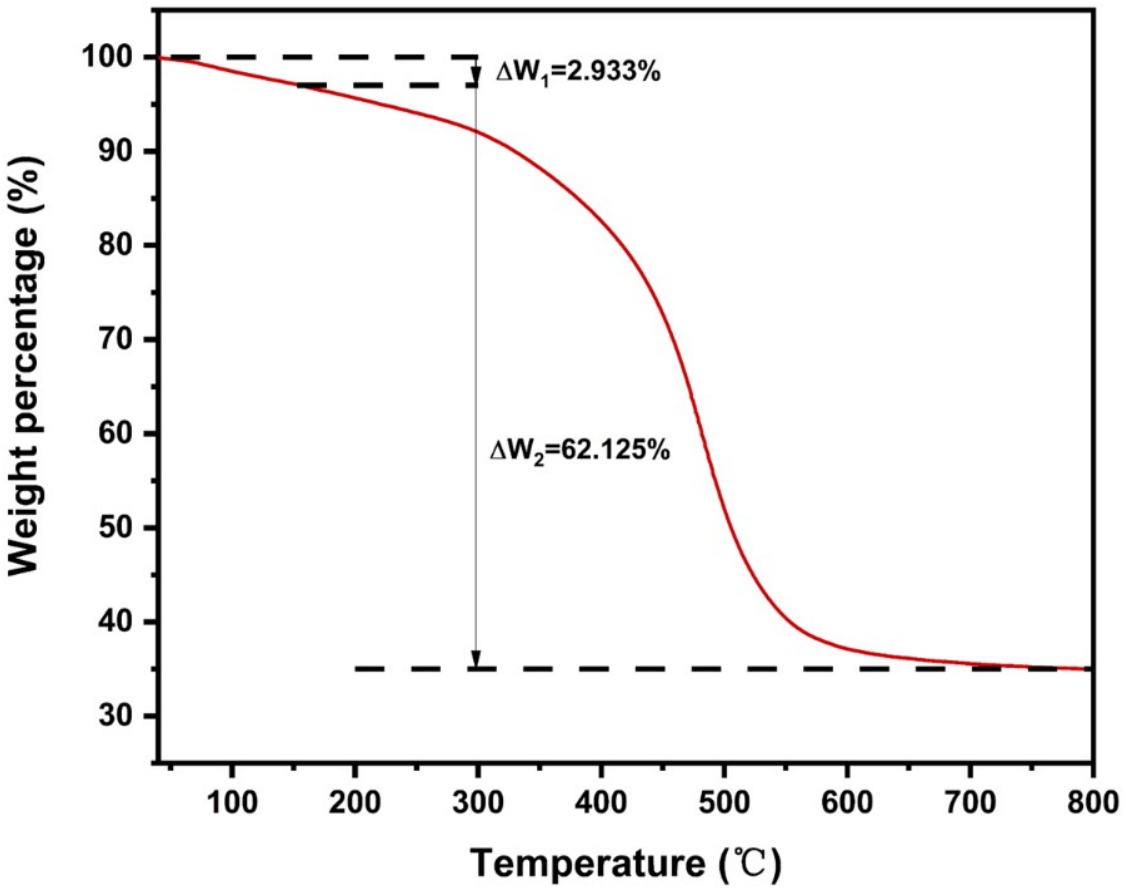

Figure S15 TGA pattern of PFCC-Hf.

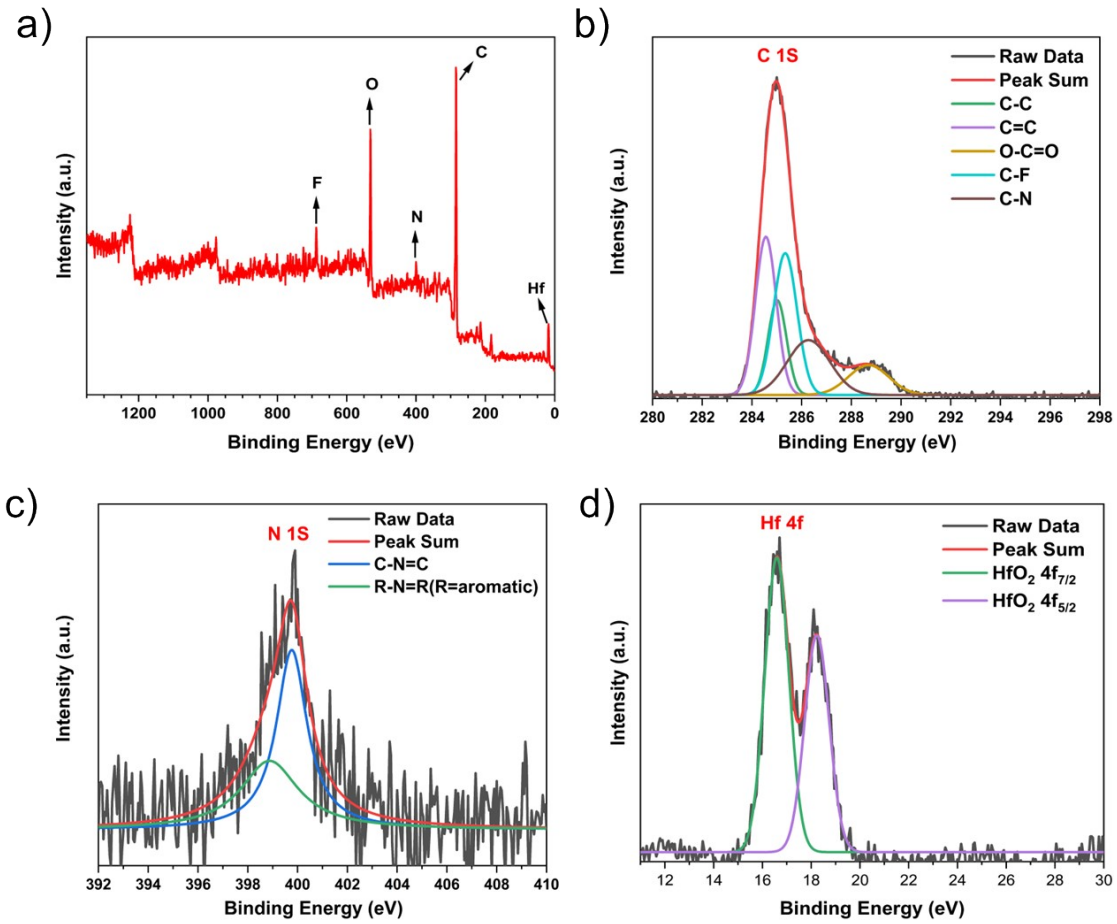

Figure S16 a) X-ray photoelectron spectroscopy (XPS) of PFCC-Hf. b) High-resolution XPS spectrum of C 1s for PFCC-Hf. c) High-resolution XPS spectrum of N 1s for PFCC-Hf. d) High-resolution XPS spectrum of Hf 4f for PFCC-Hf.

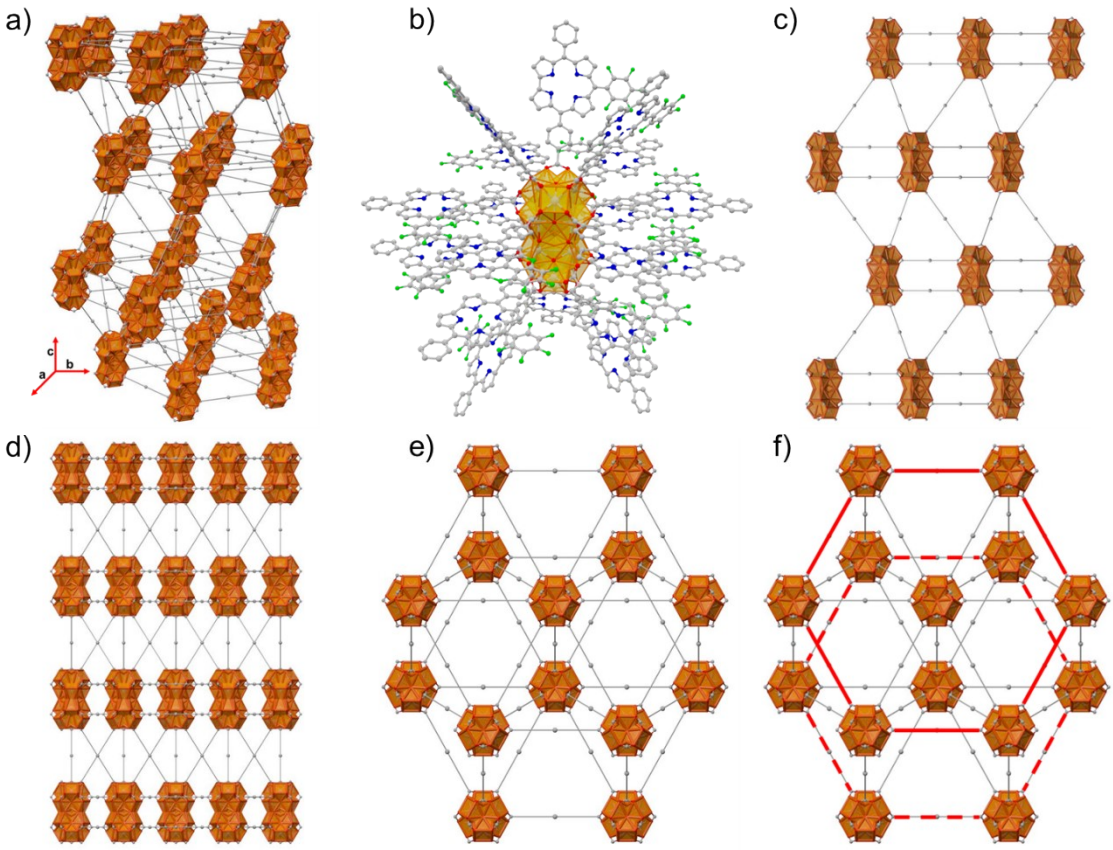

Figure S17 a) Schematic structure of the PFCC-Hf. b) Diagram of secondary building units (SBU) of PFCC-Hf simulated by $Hf_{12}(\mu_3\text{-}O)_8(\mu_3\text{-}OH)_8(\mu_2\text{-}OH)_6$ and ligand PFCC. c) View along *a* axis of the PFCC-Hf, d) view along *b* axis of the PFCC-Hf and, e) f) view along *b* axis of the PFCC-Hf. The top perspective of PFCC-Hf corresponds to the inverse FFT image of PFCC-Hf.

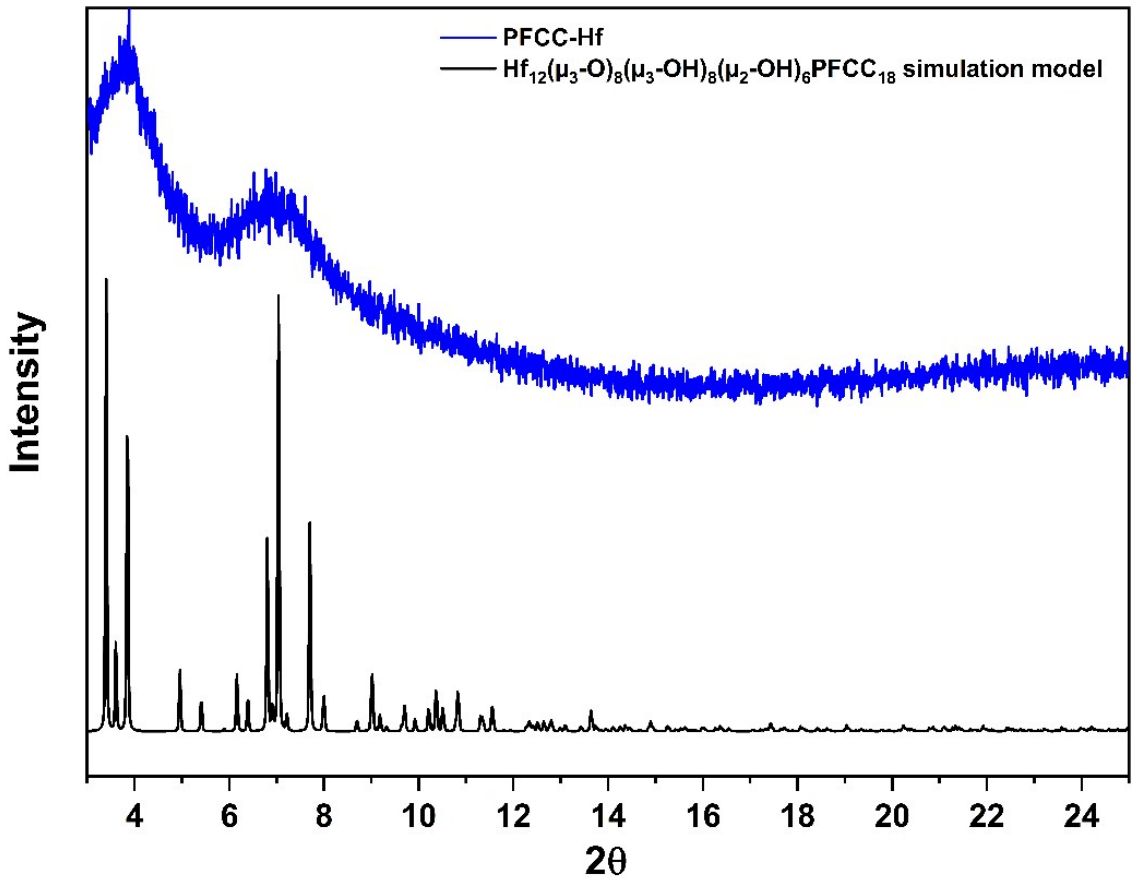

Figure S18 The PXRD of PFCC-Hf and $Hf_{12}(\mu_3\text{-}O)_8(\mu_3\text{-}OH)_8(\mu_2\text{-}OH)_6PFCC_{18}$ SBUs simulated model.

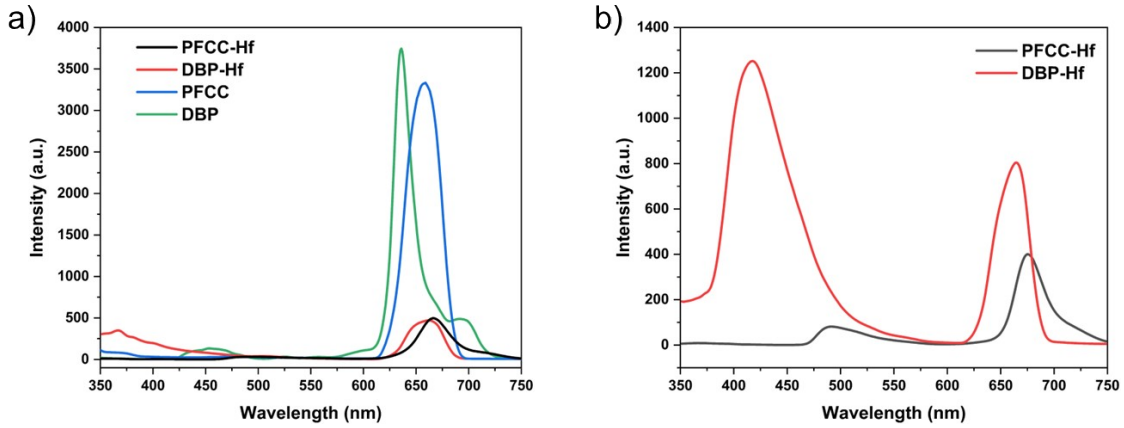

Figure S19 a) Fluorescence emission spectra of PFCC-Hf, DBP-Hf, PFCC and DBP in DMF. b) Fluorescence emission spectra of the aqueous dispersion of PFCC-Hf and DBP-Hf.

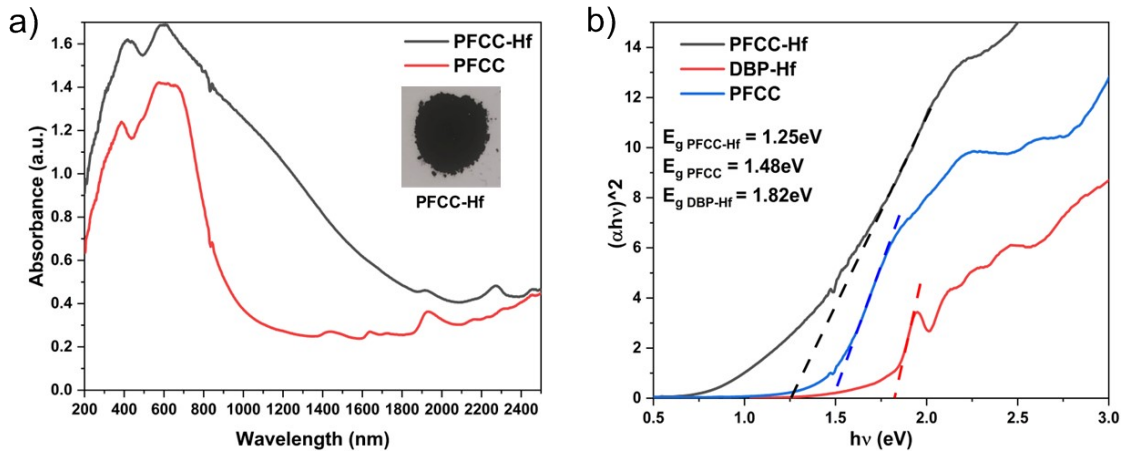

Figure S20 a) UV-Vis-RDS of PFCC-Hf and PFCC. b) Tauc plot fitted from UV-Vis-RDS data.

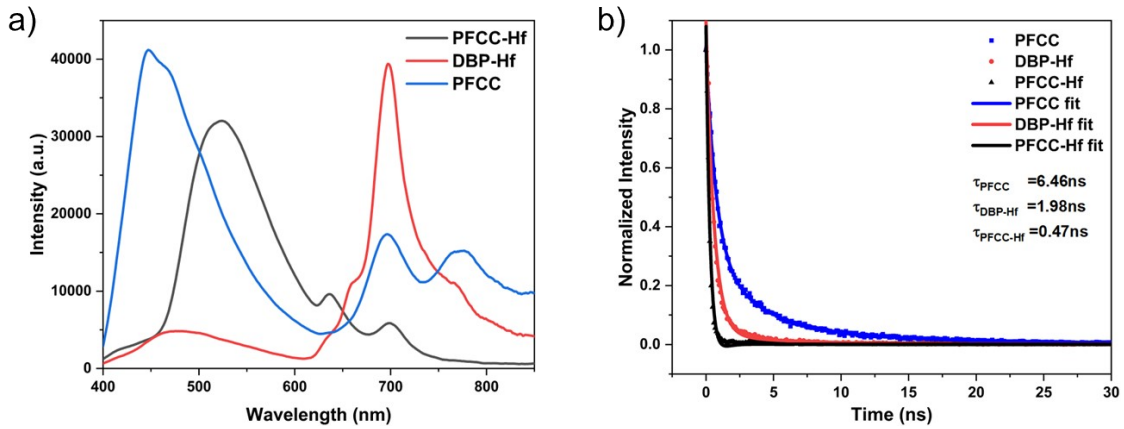

Figure S21 a) Steady-state photoluminescence spectra of PFCC-Hf, PFCC and DBP-Hf (excition:375 nm). b) Fluorescence lifetime decay fitting curve.

Table S1 Photophysical properties of PFCC-Hf and DBP-Hf. The fluorescence quantum yield (Φ_F) was measured with A Quantaurus-QY spectrometer. Non-radiative rate constant $k_{nr} = (1 - \Phi_F)/\tau$, $k_r = \Phi_F/\boldsymbol{\tau}$.

	PFCC-Hf	DBP-Hf
Φ_F	0.06	0.13
τ (ns)	0.47	1.98
k_{nr} ***(s^{-1})***	1.92×10^{9}	4.39×10^{8}
k_r ***(s^{-1})***	1.28×10^{8}	6.57×10^{7}

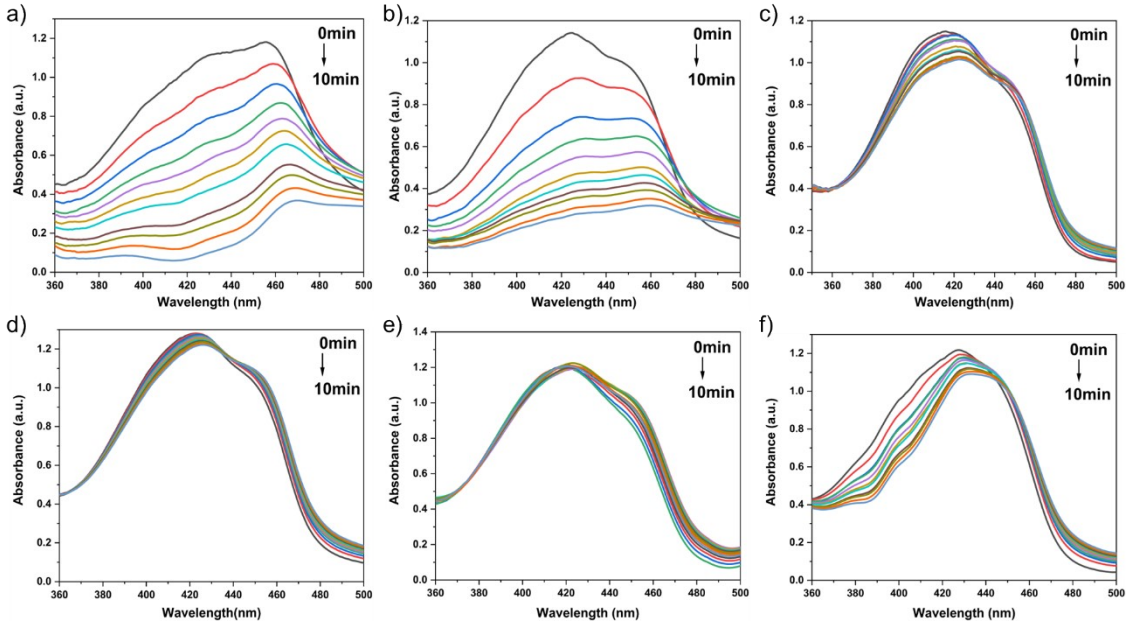

Figure S22 UV spectra of a DPBF solution mixed with 200 μg/ml of a) PFCC-Hf, b) DBP-Hf, c) PFCC, d) nothing being irradiated with a 660 nm laser for 10min, and DPBF solution mixed with 200 μg/ml of a) PFCC-Hf, b) DBP-Hf without light for 10 mins

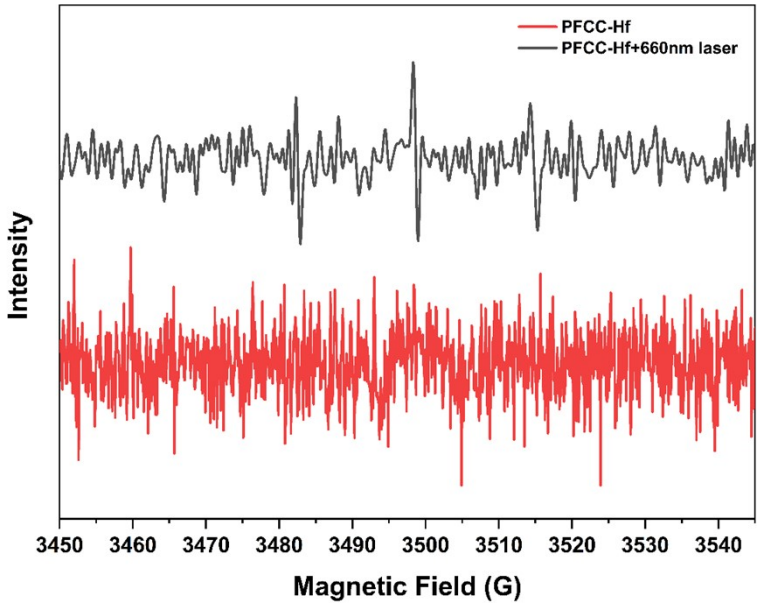

Figure S23 EPR spectra of PFCC-Hf dispersions obtained under dark conditions and irradiated with a 660 nm laser for 5 min, using TMPO as a $^1O_2$ radical trapping agent.

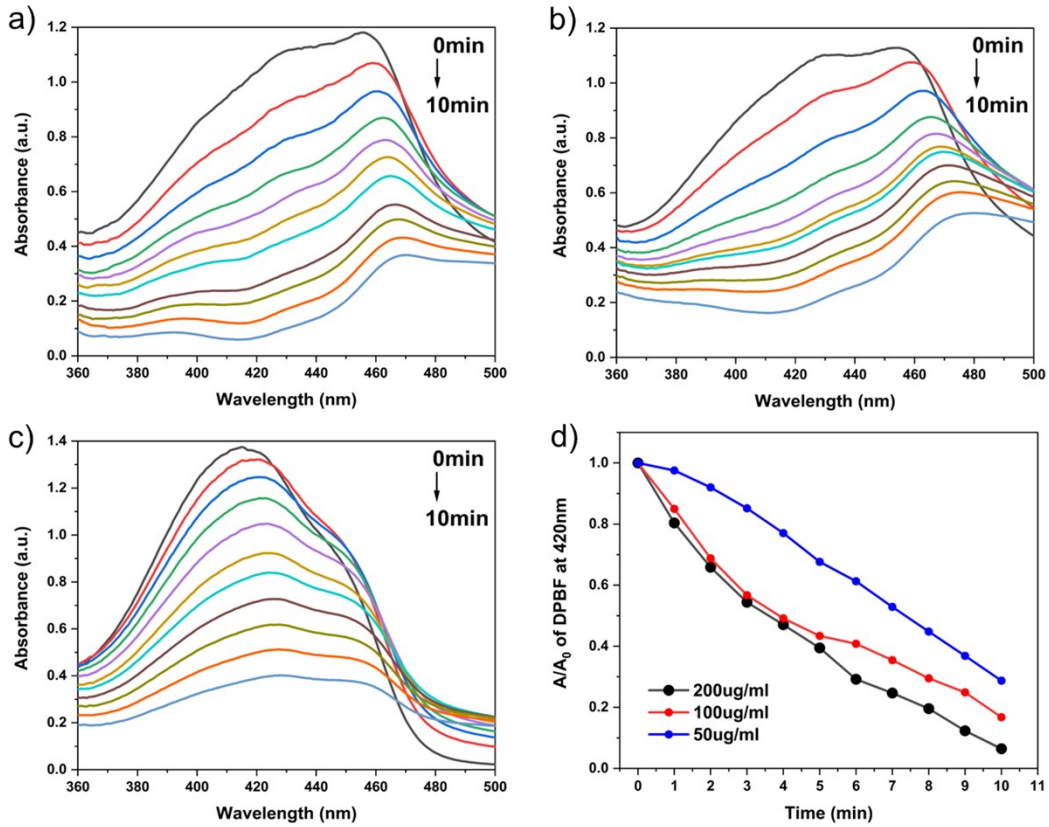

Figure S24 UV spectra of a DPBF solution mixed with a) 200 μg/ml, b) 100 μg/ml and c) 50 μg/ml of PFCC-Hf being irradiated with a 660 nm laser for 10 min. d) Time-dependent absorption (420 nm) plot of DBPF solution blended with different concentrations of PFCC-Hf under 660 nm laser exposure.

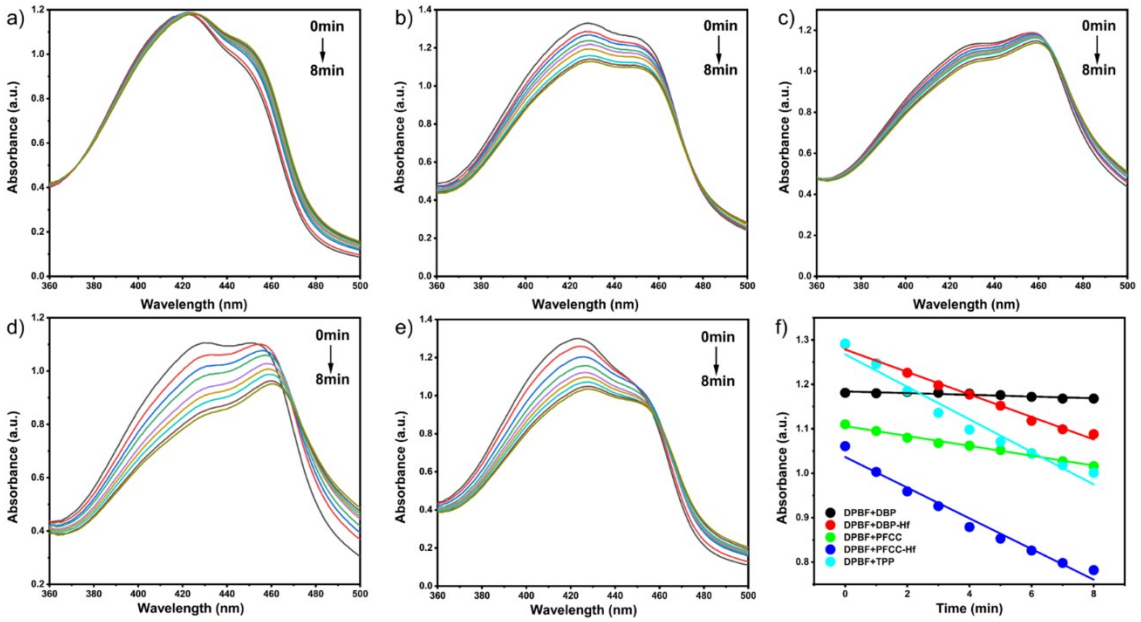

Figure S25 UV spectra of a DPBF solution mixed with 10 μM a) DBP, b) DBP-Hf, c) PFCC, d) PFCC-Hf, e) 5,10,15,20-tetraphenylporphyrin (TPP) being irradiated with a 660 nm laser for 8 min, where the molar quantities of PFCC-Hf and DBP-Hf were calculated with a PFCC/DBP: Hf ratio of 0.56. f) Absorbance-time curve at 420 nm of DPBF solutions mixed with photosensitizers exposure to 660 nm laser.

Table S2 $^1O_2$ quantum yields of different photosensitizers under 660 nm illumination with TPP as reference. ***k*** represents the slope of absorbance-time curve at 420 nm of DPBF. **OD** represents the absorbance of different photosensitizers at 660nm. $\boldsymbol{\Phi_\Delta}$ represent the singlet oxygen quantum yields of the photosensitizers.

Photosensitizer	**DBP**	**DBP-Hf**	**PFCC**	**PFCC-Hf**	**TPP**
k	-0.00192	-0.0253	-0.0111	-0.0345	-0.03659
OD	0.039	0.227	0.554	0.175	0.1
Φ_Δ	0.0804	0.2236	0.0554	0.3742	0.64

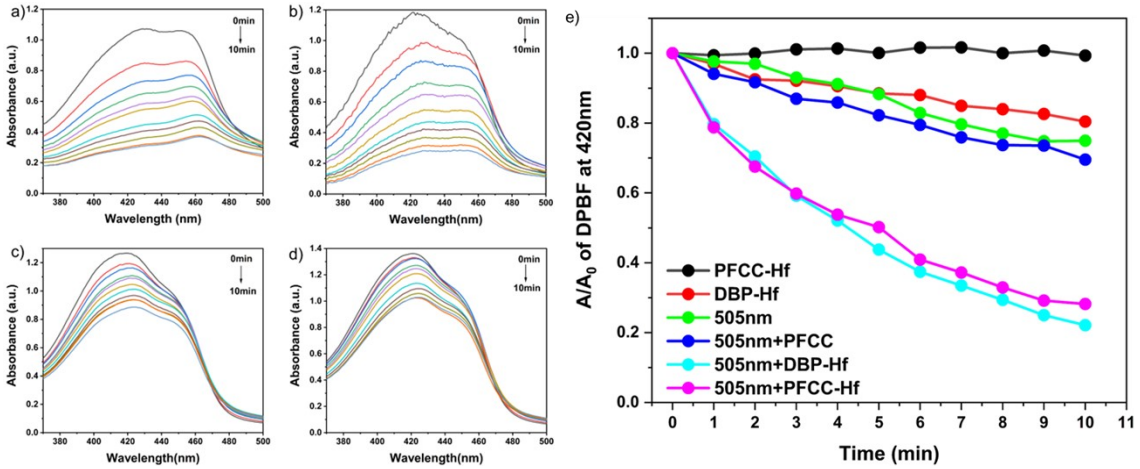

Figure S26 UV spectra of a DPBF solution mixed with 200 μg/ml of a) PFCC-Hf, b) DBP-Hf, c) PFCC, d) nothing under 505 nm irradiation for 10 min. e) Time-dependent absorption (420 nm) patterns of aqueous solutions of DBPF with different treatment.

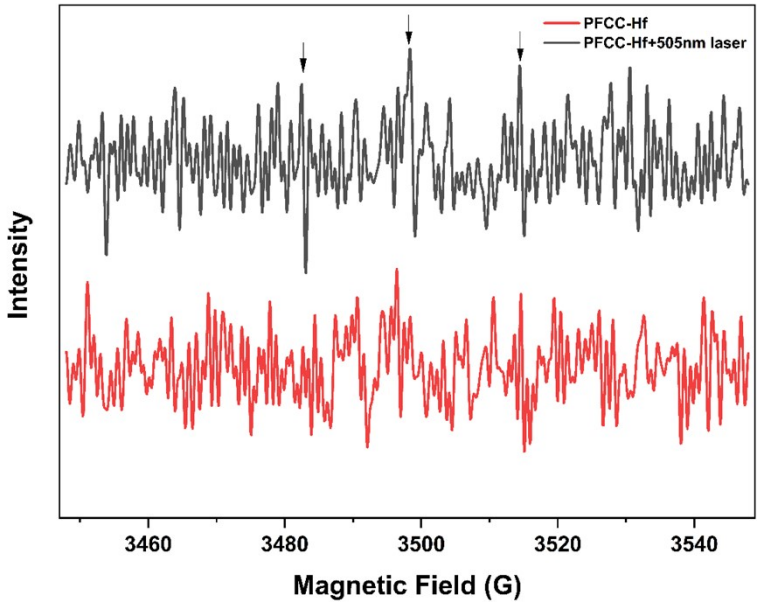

Figure S27 EPR spectra of PFCC-Hf dispersions were obtained in the dark and irradiated with a 505 nm laser exposure for 5 min, with TMPO acting as a $^1O_2$ radical trapping agent.

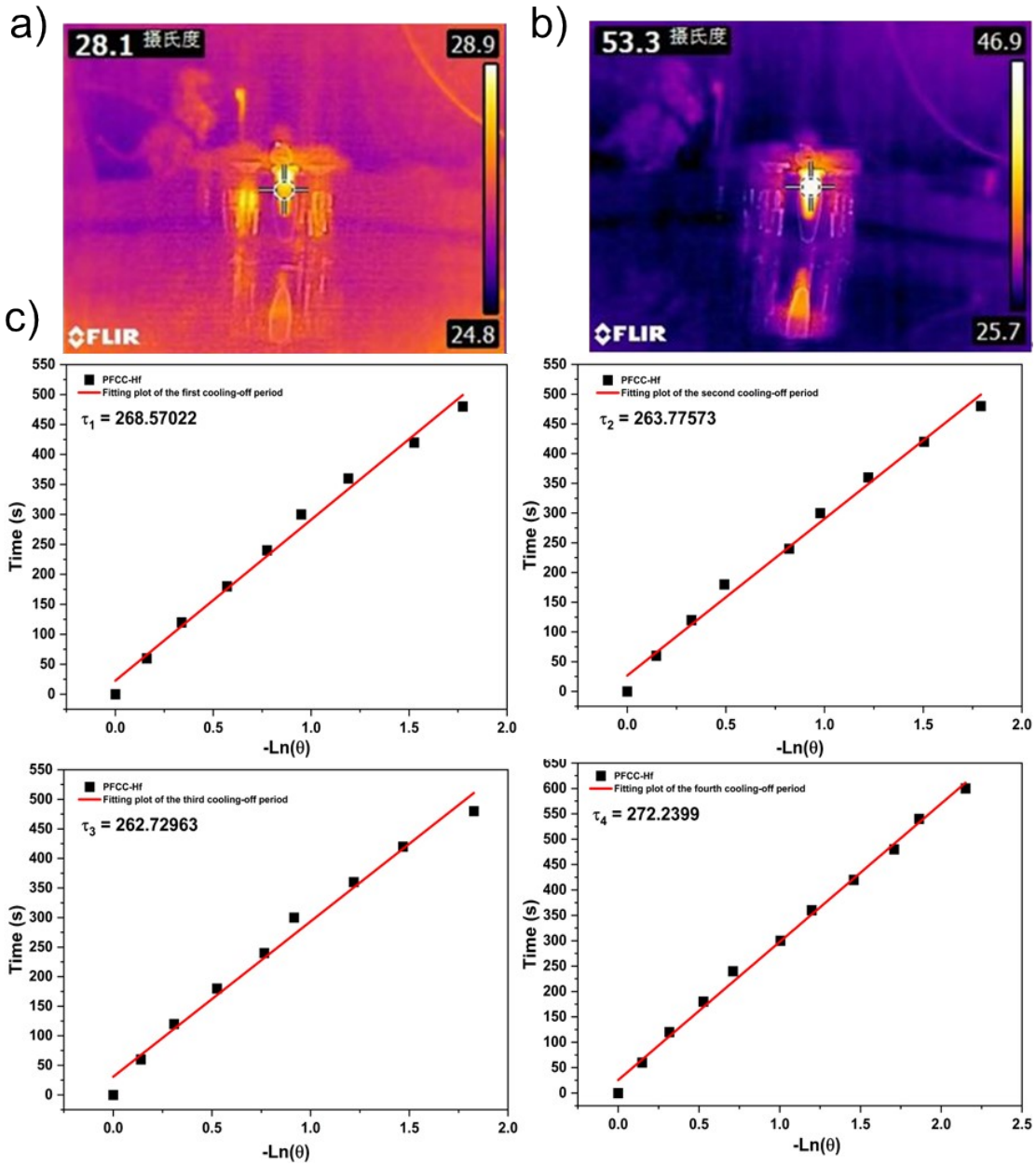

Figure S28 Temperature images of PFCC-Hf a) initiation and, b)10 min after 808 nm laser (1W/cm^2) treatment captured by the thermal infrared imager. c) Graphs exhibiting cooling time against the constant -Ln(θ) acquired from the 4 cycles of cooling stage of PFCC-Hf. The final Time parameters τ_S was the average of the data values obtained from the 4 cycles.

Table S3 Comparison of the photothermal conversion efficiency of reported nano-photothermal agents and PFCC-Hf.

PTT Materials	conversion efficiency / %	Reference
NanoPcAF	18.3	9
CPF-Cu	39.3	10
BP-AuNSs	28.4	11
BQDs	23.7	12
DPP2+NPs	35.0	13
FeCUPs	47.4	14
Fe-EA	17.1	15
Co2C-PEG	37.5	16
GNRs@PDA-BTS	34.6	17
MnGdOP@PDA-PEG	21.5	18
Py@Ca-NDI	41.8	19
BTPPA+PAE	60.0	20
Tfm-BDP	88.3	21
PFCC-Hf	**44.6**	**This work**

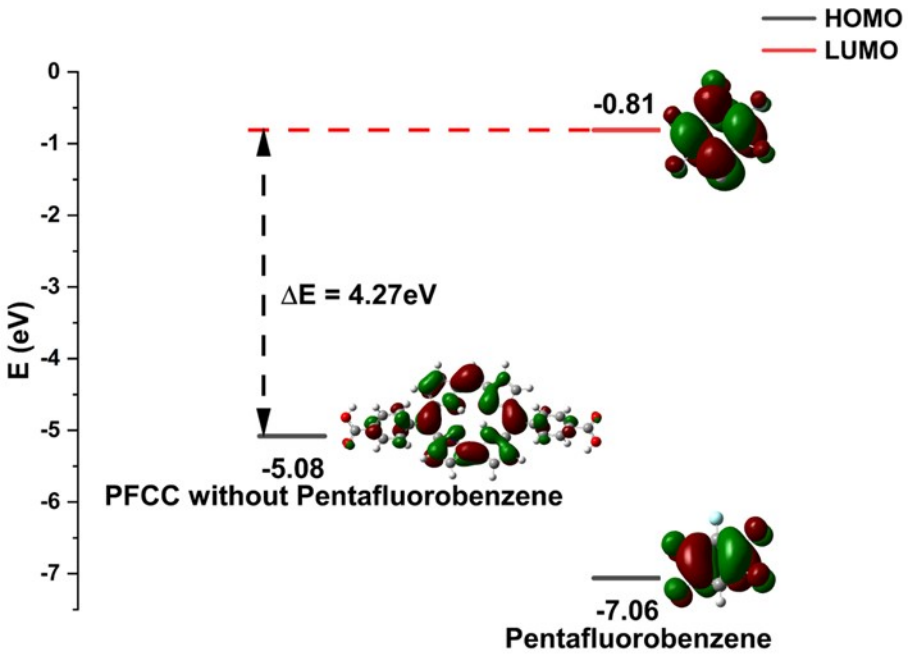

Figure S29 Scheme of the frontier molecular orbital energy levels of the pentafluoro benzene and the electron-donor part of the corrole molecular PFCC.

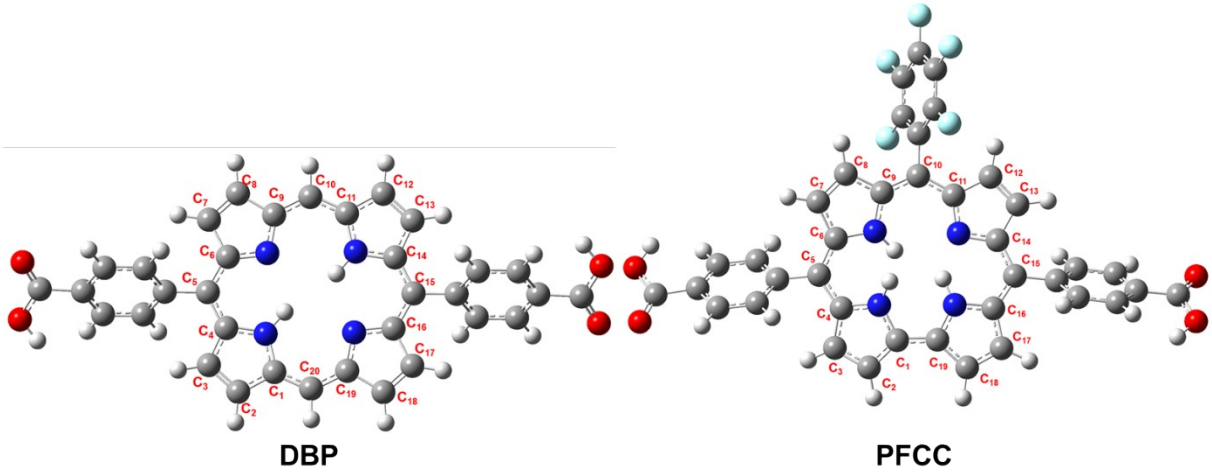

Figure S30 Diagram of the molecular configurations of PFCC and DBP.

Table S4 Dihedral angles of the carbocyclic in PFCC and DBP.

dihedral angle	Porphyrin ligand PFCC	dihedral angle	Corrolic ligand PFCC
∠C_1-C_2-C_{18}-C_{19}	179.05	∠C_1-C_2-C_{18}-C_{19}	17.36
∠C_3-C_4-C_6-C_7	13.31	∠C_3-C_4-C_6-C_7	77.72
∠C_8-C_9-C_{11}-C_{12}	1.20	∠C_8-C_9-C_{11}-C_{12}	16.97
∠C_{13}-C_{14}-C_{16}-C_{17}	13.31	∠C_{13}-C_{14}-C_{16}-C_{17}	41.09

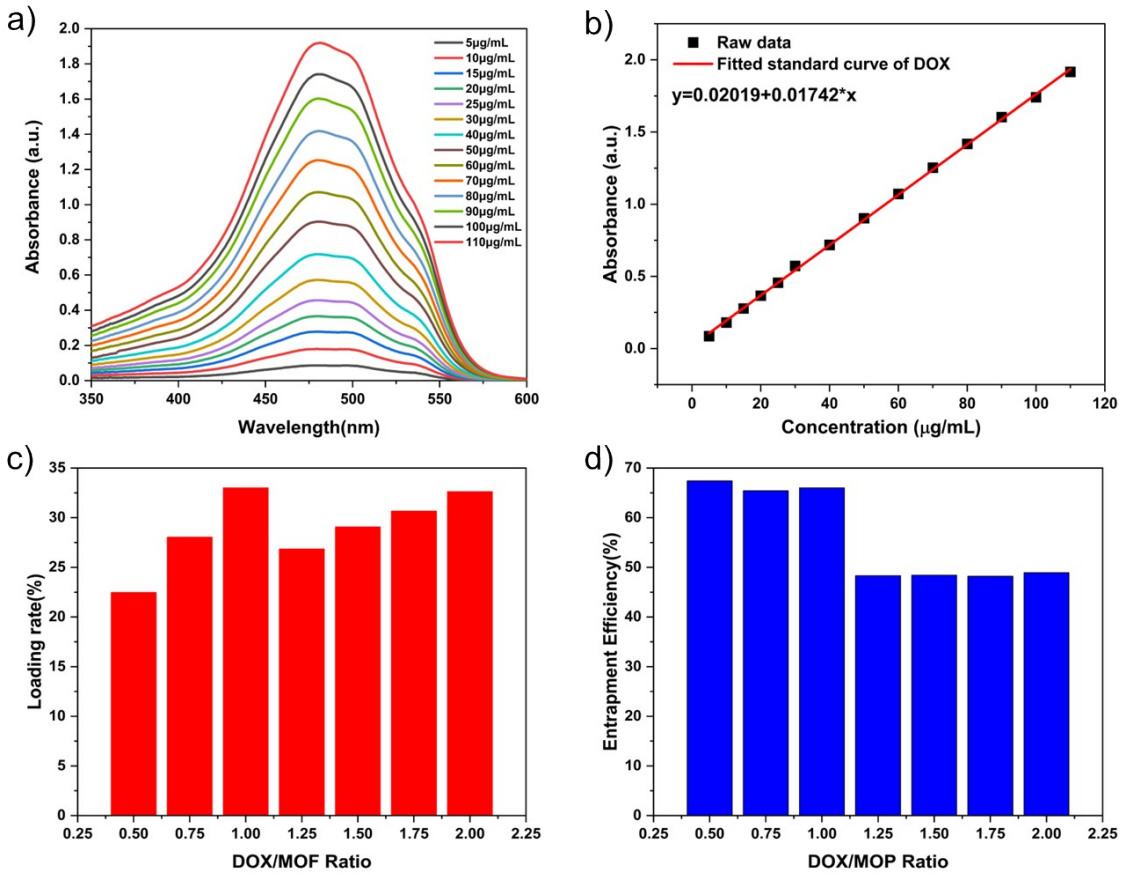

Figure S31 a) UV absorption spectra of DOX aqueous solutions. b) Standard concentration-absorbance curve for DOX. c) DOX loading rate and entrapment efficiency at different ratios of DOX/PFCC-Hf.

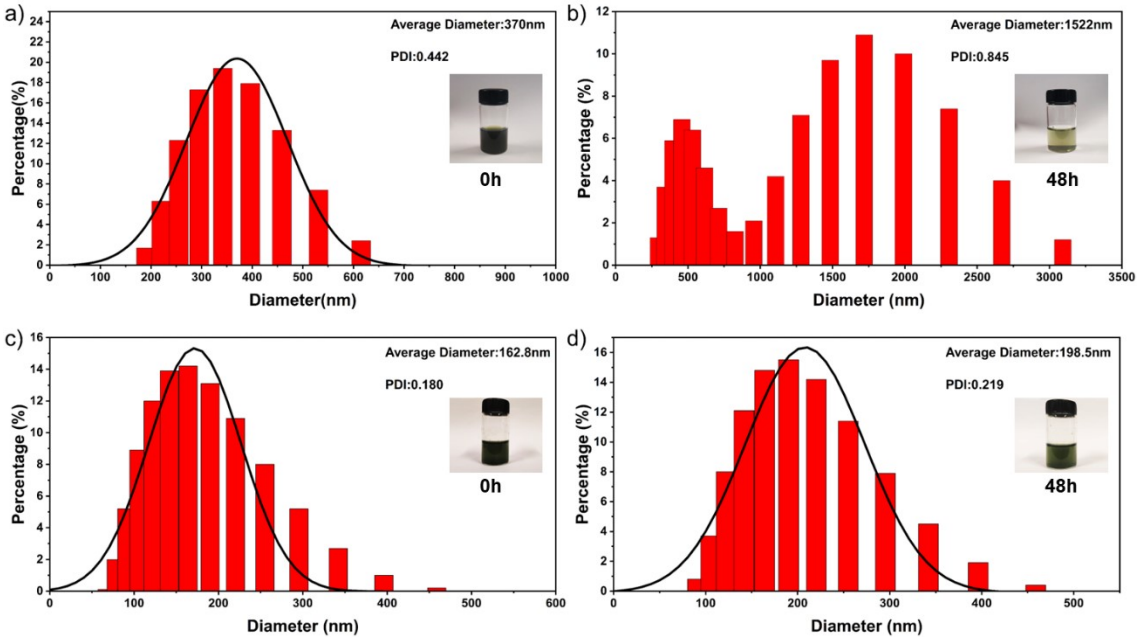

Figure S32 Dynamic light scattering (DLS) data of PFCC-Hf and PFCC-Hf@PEG in PBS buffer (pH=7.2) measured at different settling times.

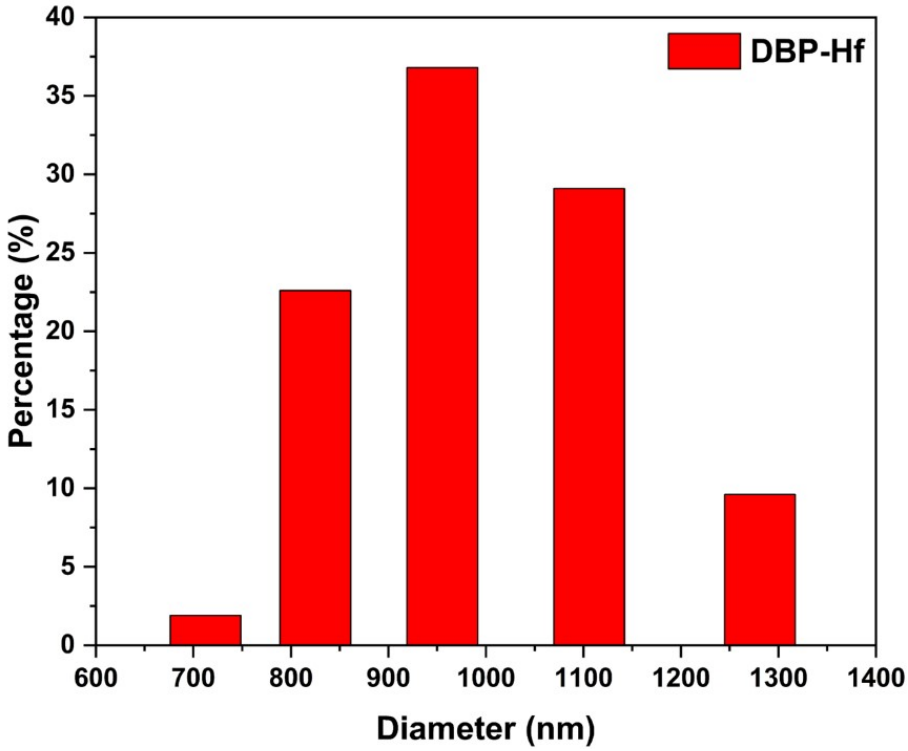

Figure S33 Particle size data of porphyrin-based MOF DBP-Hf tested in water.

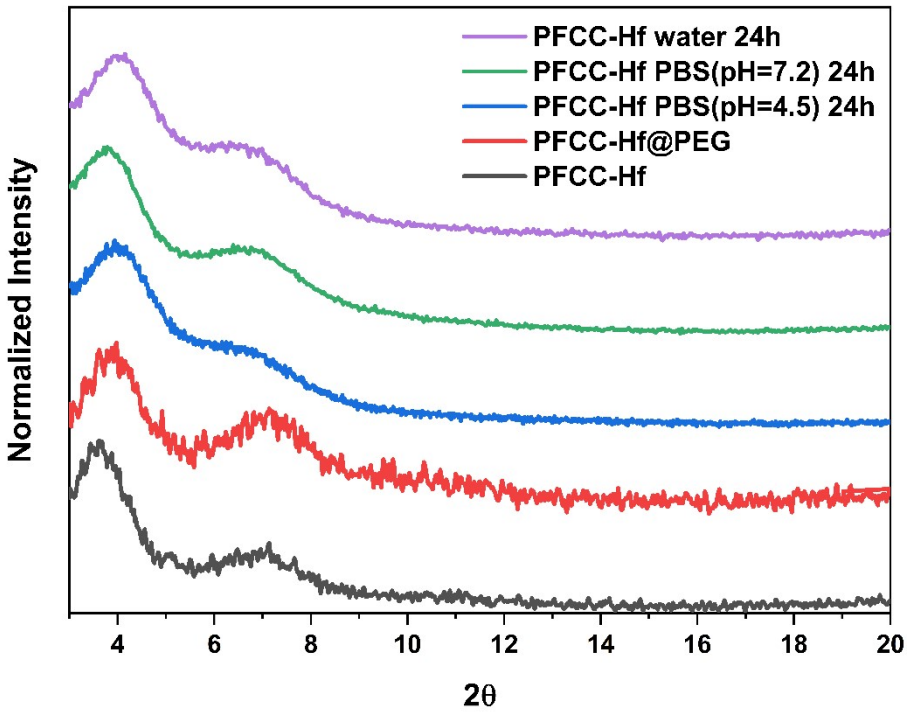

Figure S34 XRD data of PFCC-Hf before and after immersion in different solvents for 24 h, and XRD of PFCC-Hf@PEG.

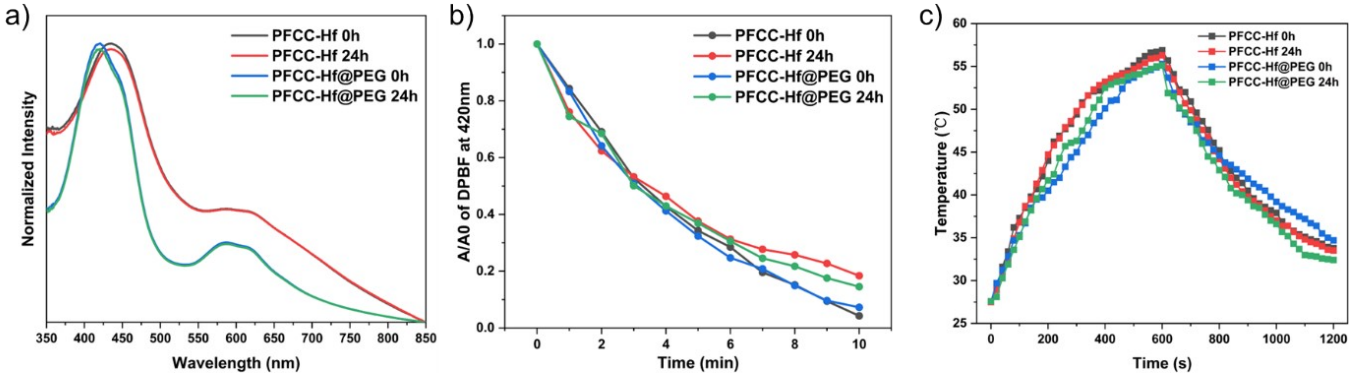

Figure S35 a) UV spectra of PFCC-Hf and PFCC-Hf@PEG after immersion in PBS buffer (pH=7.2) for 24 h. Validation of b) PDT and c) PTT effects of PFCC-Hf and PFCC-Hf@PEG after

24h soaking in PBS buffer (pH=7.2) for 24 h, while the concentration of the two materials was 200 μg/mL.

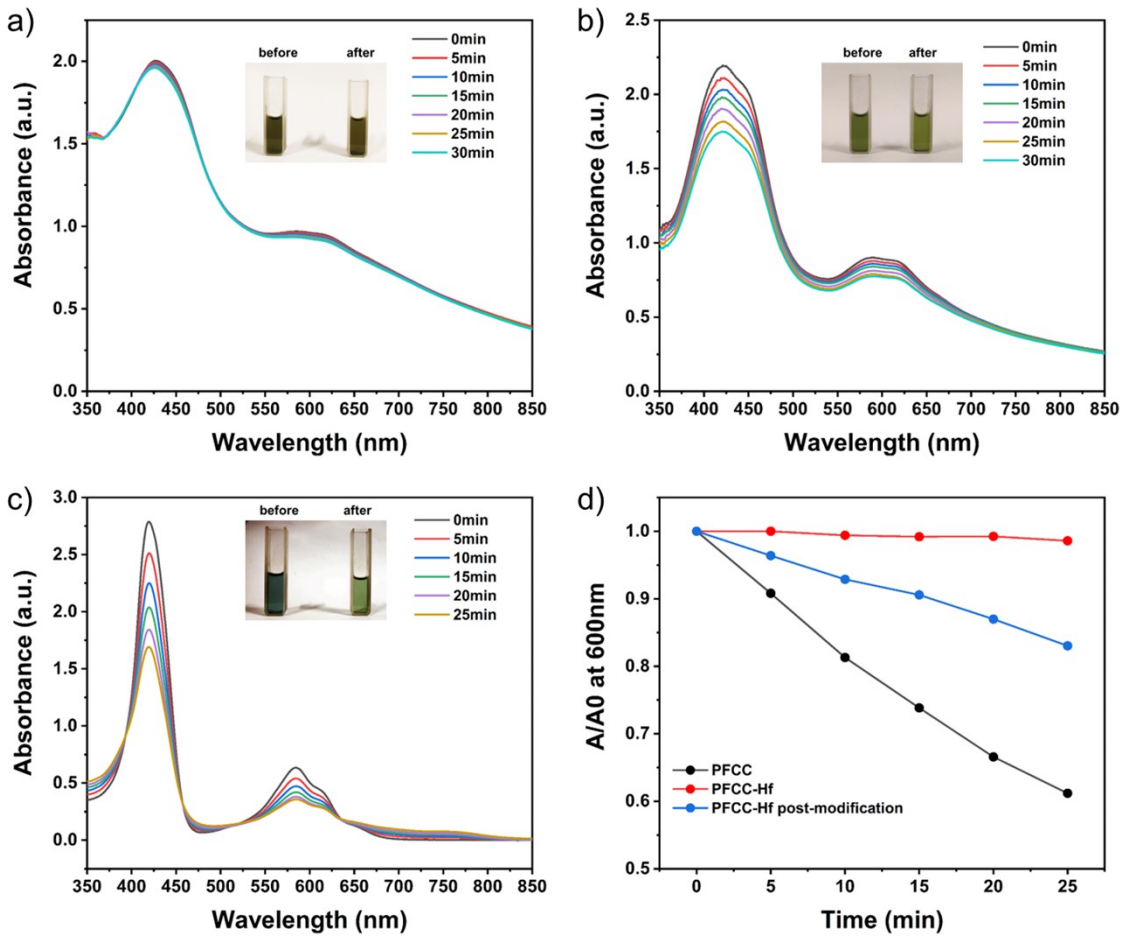

Figure S36 UV-vis absorption of a) PFCC-Hf in water, b) PFCC-Hf@PEG in water and c) PFCC in DMF solutions before and after 660 nm laser irradiation (0.1W/cm^2). d) Absorbance at 600 nm versus 660 nm illumination time for photosensitive materials.

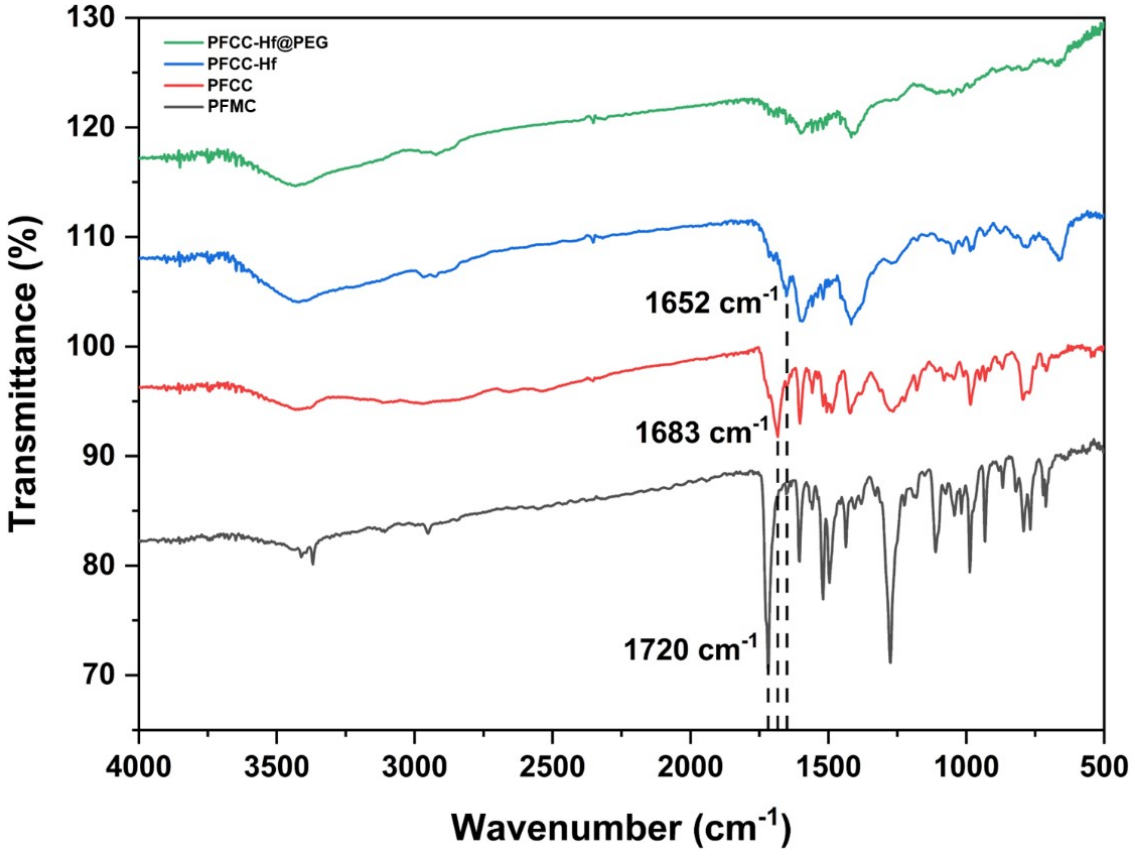

Figure S37 Infrared (IR) spectra of PFMC, PFCC, PFCC-Hf and PFCC-Hf@PEG, where the IR absorption peak of PFMC at 1720 cm^{-1} corresponds to the ester group of PFMC, the IR absorption peak of PFCC at 1683 cm^{-1} corresponds to the carboxyl group of PFCC, and the IR absorption peak of PFCC-Hf at 1652 cm^{-1} corresponds to the carboxylate of PFCC-Hf.

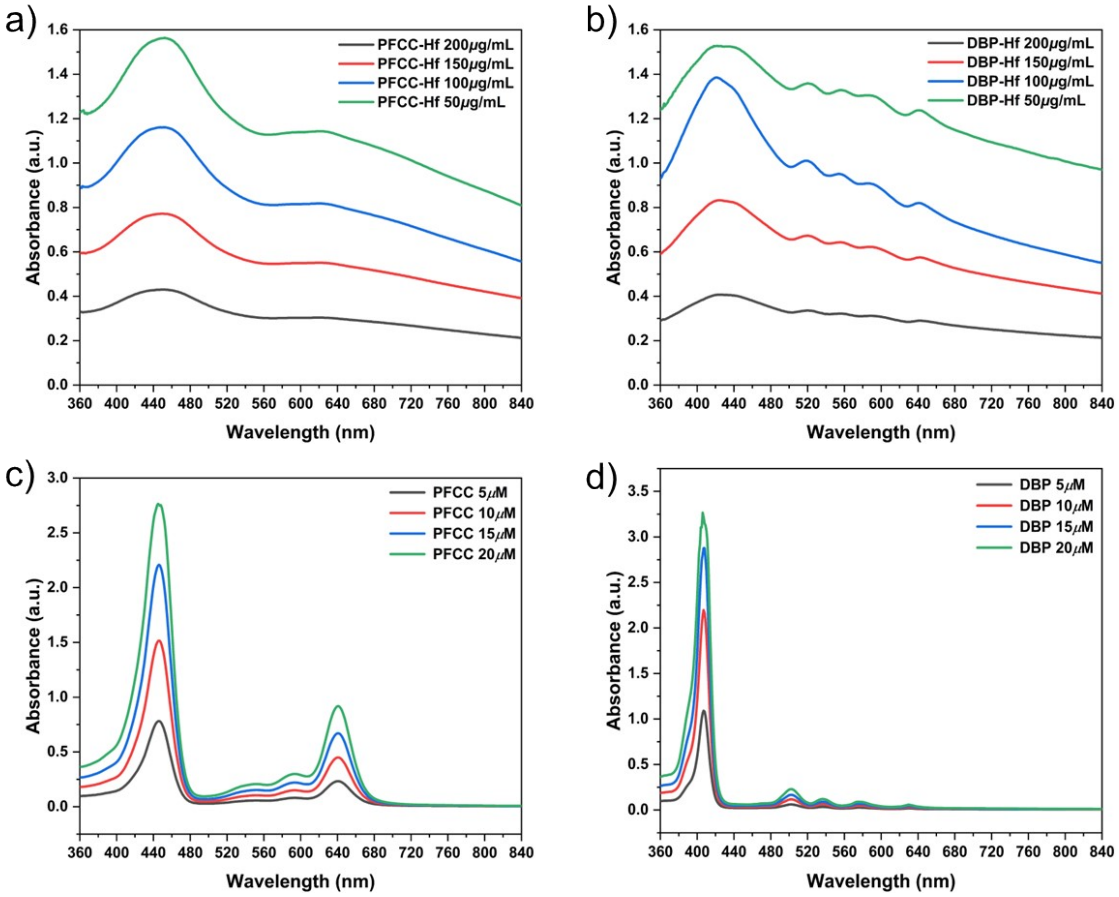

Figure S38 UV of aqueous dispersions with different concentrations of PFCC-Hf, DBP-Hf, PFCC and DBP.

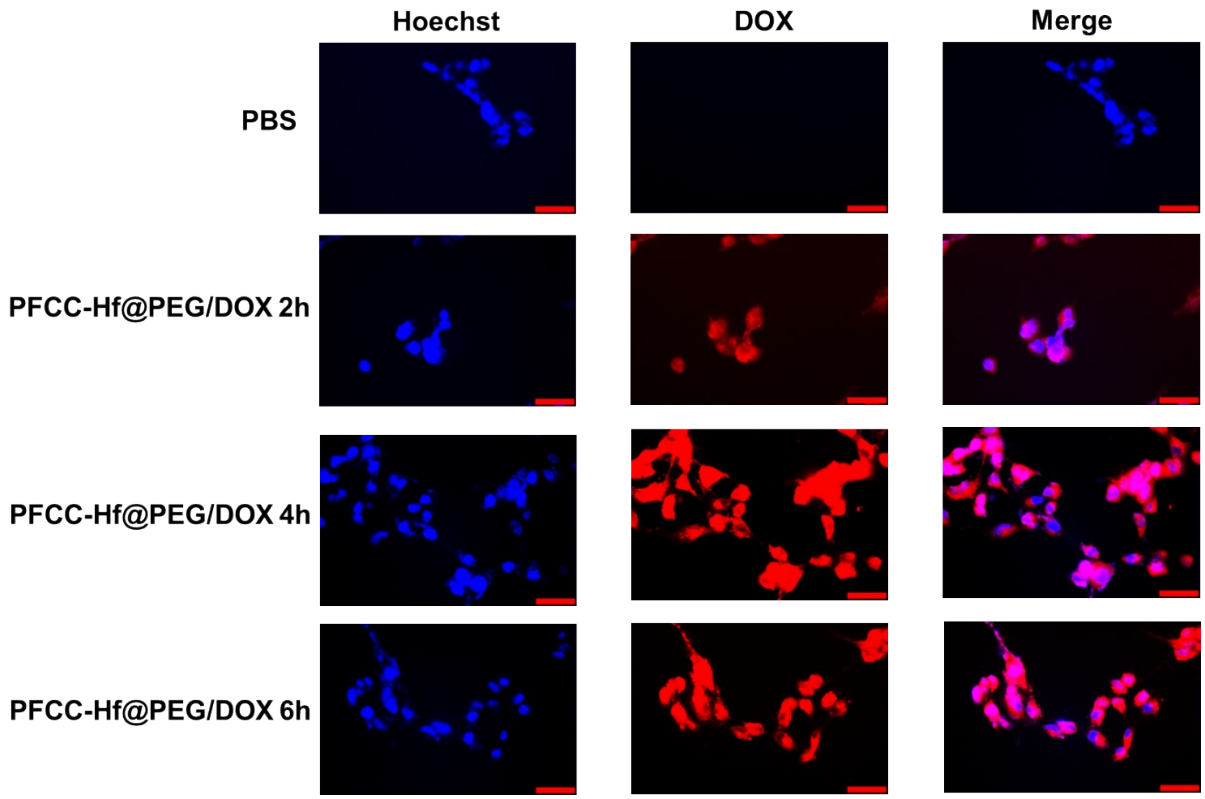

Figure S39 Fluorescence imaging of uptake of A375 cells for PFCC-Hf@PEG against incubation time. Scale bar: 50 μm.

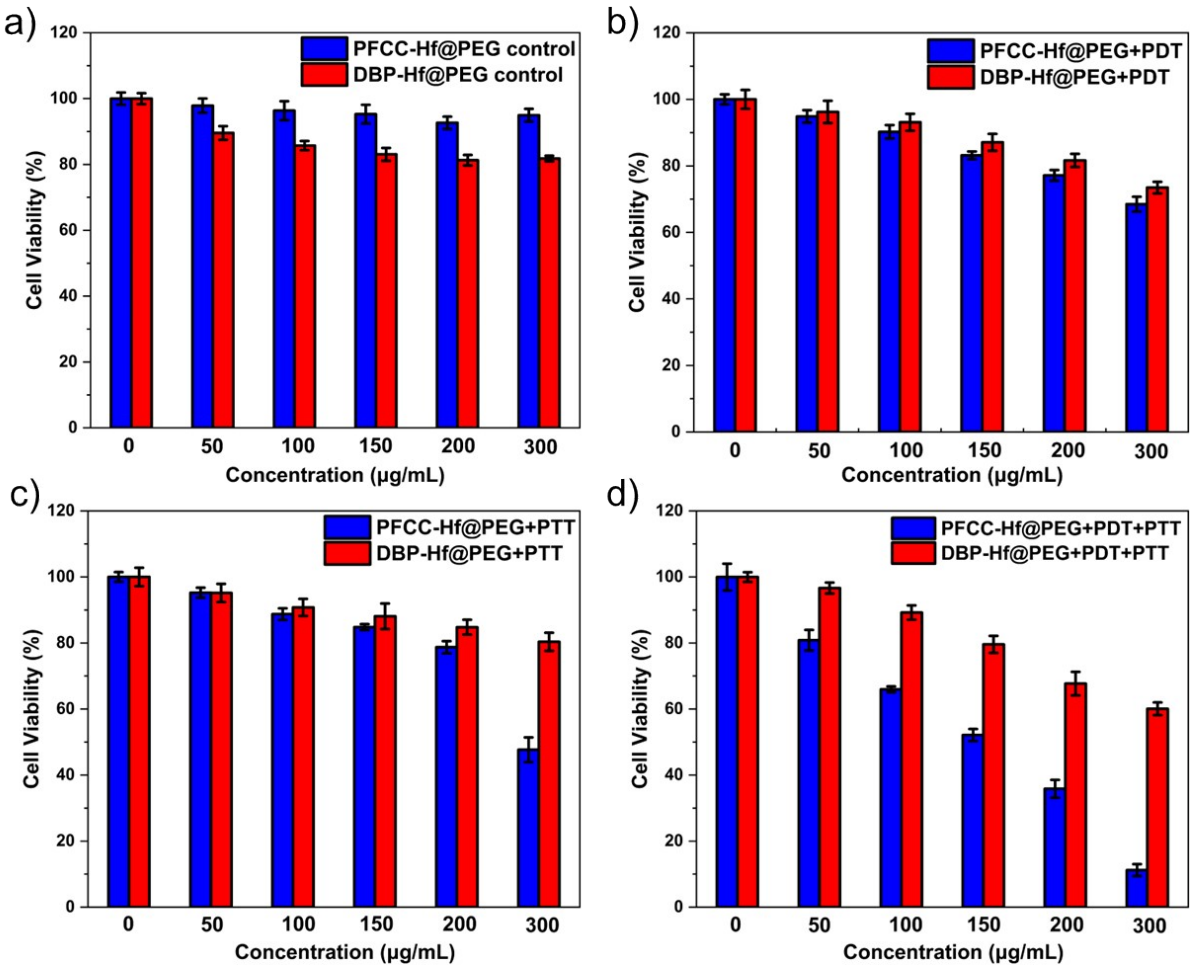

Figure S40 *In vitro* cytotoxicity testing of PFCC-Hf@PEG and DBP-Hf@PEG in conditions with and without laser irradiation, where PDT refers to 660nm laser irradiation, PTT refers to 808nm laser irradiation.

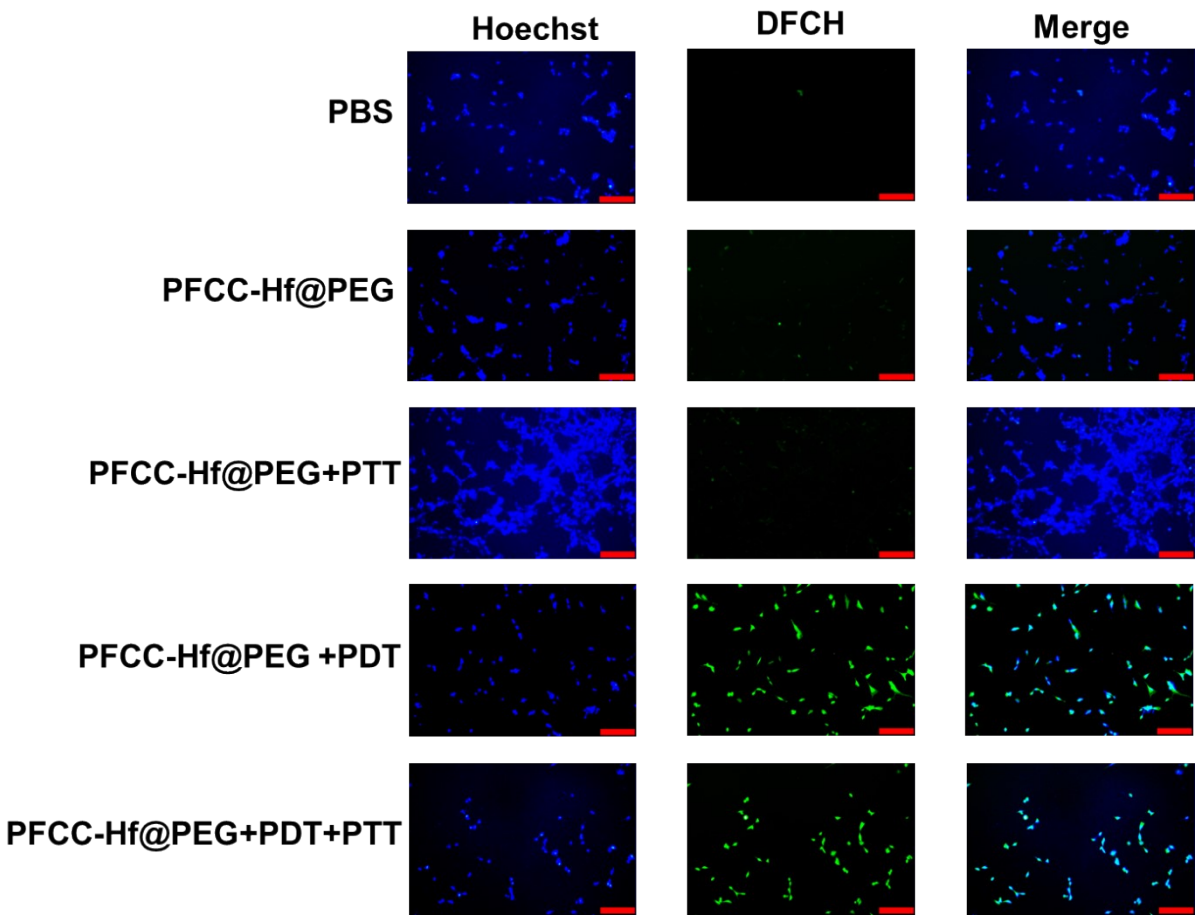

Figure S41 Fluorescence imaging of detecting ROS generated by PFCC-Hf@PEG PDT effect using DFCH-DA. Scale bar: 200 μm.

REFERENCES

1. C. Brückner, Y. Zhang, S. J. Rettig and D. Dolphin, Synthesis, derivatization and structural characterization of octahedral tris(5-phenyl-4,6-dipyrrinato) complexes of cobalt(III) and iron(III), *Inorganica Chimica Acta*, 1997, **263**, 279-286.
2. T. Rohand, E. Dolusic, T. H. Ngo, W. Maes and W. Dehaen, Efficient synthesis of aryldipyrromethanes in water and their application in the synthesis of corroles and dipyrromethenes, *Arkivoc*, 2007, 307-324.
3. J. M. Wang, Y. Li, H. Q. Yuan, D. H. Wu, X. Ying, L. Shi, H. T. Zhang and H. Y. Liu, Methyl Benzoate Gallium(III) corrole complexes: DNA-binding, Photocleavage Activity, Cytotoxicity on Tumor Cells, *Appl. Organomet. Chem.*, 2017, **31**, 12.
4. K. D. Lu, C. B. He and W. B. Lin, Nanoscale Metal-Organic Framework for Highly Effective Photodynamic Therapy of Resistant Head and Neck Cancer, *J. Am. Chem. Soc.*,

2014, **136**, 16712-16715.
5. L. Wang, X. Z. Qu, Y. X. Zhao, Y. Z. W. Weng, G. I. N. Waterhouse, H. Yan, S. Y. Guan and S. Y. Zhou, Exploiting Single Atom Iron Centers in a Porphyrin-like MOF for Efficient Cancer Phototherapy, *ACS Appl. Mater. Interfaces*, 2019, **11**, 35228-35237.
6. S. Meng, Z. P. Xu, G. Hong, L. H. Zhao, Z. J. Zhao, J. H. Guo, H. Y. Ji and T. J. Liu, Synthesis, characterization and in vitro photodynamic antimicrobial activity of basic amino acid-porphyrin conjugates, *Eur. J. Med. Chem.*, 2015, **92**, 35-48.
7. M. Q. Yang, J. R. Deng, D. Guo, J. Zhang, L. X. Yang and F. S. Wu, A folate-conjugated platinum porphyrin complex as a new cancer-targeting photosensitizer for photodynamic therapy (vol 17, pg 5367, 2019), *Org. Biomol. Chem.*, 2020, **18**, 569-569.
8. D. K. Roper, W. Ahn and M. Hoepfner, Microscale heat transfer transduced by surface plasmon resonant gold nanoparticles, *J. Phys. Chem. C*, 2007, **111**, 3636-3641.
9. Y. Y. Zhao, L. Zhang, Z. X. Chen, B. Y. Zheng, M. R. Ke, X. S. Li and J. D. Huang, Nanostructured Phthalocyanine Assemblies with Efficient Synergistic Effect of Type I Photoreaction and Photothermal Action to Overcome Tumor Hypoxia in Photodynamic Therapy, *J. Am. Chem. Soc.*, 2021, **143**, 13980-13989.
10. B. J. Li, Y. K. Lv, Z. D. Wang, P. Peng and S. Q. Zang, Edge confined covalent organic framework with efficient biocompatibility and photothermic conversion, *Nano Today*, 2021, **37**, 9.
11. G. C. Yang, Z. M. Liu, Y. Li, Y. Q. Hou, X. X. Fei, C. K. Su, S. M. Wang, Z. F. Zhuang and Z. Y. Guo, Facile synthesis of black phosphorus-Au nanocomposites for enhanced photothermal cancer therapy and surface-enhanced Raman scattering analysis, *Biomater. Sci.*, 2017, **5**, 2048-2055.
12. T. Guo, Q. Y. Tang, Y. T. Guo, H. L. Qiu, J. Dai, C. Xing, S. H. Zhuang and G. M. Huang, Boron Quantum Dots for Photoacoustic Imaging-Guided Photothermal Therapy, *ACS Appl. Mater. Interfaces*, 2021, **13**, 306-311.
13. C. N. Li, W. Zhang, S. Liu, X. L. Hu and Z. G. Xie, Mitochondria-Targeting Organic Nanoparticles for Enhanced Photodynamic/Photothermal Therapy, *ACS Appl. Mater. Interfaces*, 2020, **12**, 30077-30084.
14. J. X. Wang, C. J. Yao, B. Shen, X. H. Zhu, Y. Li, L. Y. Shi, Y. Zhang, J. L. Liu, Y. L. Wang and L. N. Sun, Upconversion-Magnetic Carbon Sphere for Near Infrared Light-Triggered Bioimaging and Photothermal Therapy, *Theranostics*, 2019, **9**, 608-619.
15. G. Z. Zhao, H. H. Wu, R. L. Feng, D. D. Wang, P. P. Xu, P. Jiang, K. Yang, H. B. Wang, Z. Guo and Q. W. Chen, Novel Metal Polyphenol Framework for MR Imaging-Guided Photothermal Therapy, *ACS Appl. Mater. Interfaces*, 2018, **10**, 3295-3304.
16. D. Y. Zhang, H. Xu, T. He, M. R. Younis, L. L. Zeng, H. K. Liu, C. Jiang, J. Lin and P. Huang, Cobalt carbide-based theranostic agents for in vivo multimodal imaging guided photothermal therapy, *Nanoscale*, 2020, **12**, 7174-7179.
17. Q. L. Lu, T. Lu, M. Xu, L. F. Yang, Y. L. Song and N. Li, SO2 prodrug doped nanorattles with extra-high drug payload for "collusion inside and outside" photothermal/pH triggered - gas therapy, *Biomaterials*, 2020, **257**, 14.
18. Z. H. Zhao, K. Xu, C. Fu, H. Liu, M. Lei, J. F. Bao, A. L. Fu, Y. Yu and W. G. Zhang, Interfacial engineered gadolinium oxide nanoparticles for magnetic resonance imaging guided microenvironment-mediated synergetic chemodynamic/photothermal therapy, *Biomaterials*, 2019, **219**, 12.
19. L. Zeng, L. Huang, Z. H. Wang, J. W. Wei, K. Huang, W. H. Lin, C. Y. Duan and G. Han,

Self-Assembled Metal-Organic Framework Stabilized Organic Cocrystals for Biological Phototherapy, *Angew. Chem.-Int. Edit.*, 2021, **60**, 23569-23573.
20. J. Li, J. X. Wang, J. Y. Zhang, T. Han, X. Y. Hu, M. M. S. Lee, D. Wang and B. Z. Tang, A Facile Strategy of Boosting Photothermal Conversion Efficiency through State Transformation for Cancer Therapy, *Adv. Mater.*, 2021, **33**, 9.
21. D. M. Xi, M. Xiao, J. F. Cao, L. Y. Zhao, N. Xu, S. R. Long, J. L. Fan, K. Shao, W. Sun, X. H. Yan and X. J. Peng, NIR Light-Driving Barrier-Free Group Rotation in Nanoparticles with an 88.3% Photothermal Conversion Efficiency for Photothermal Therapy, *Adv. Mater.*, 2020, **32**, 8.